GAMMA-RAY ENERGY RESPONSE OF ENCAPSULATED ^{7}LiF AND CaF_2:Mn THERMOLUMINESCENT DOSIMETERS

by

KRISHNAN LAKSHMINARAYAN

B. Tech., Indian Institute of Technology
Madras, INDIA, 1974

A MASTER'S THESIS

submitted in partial fulfillment of the

requirements of the degree

MASTER OF SCIENCE

Department of Nuclear Engineering
KANSAS STATE UNIVERSITY
Manhattan, Kansas

1980

Approved by:

G.G. Simons

Major Professor

THIS BOOK
CONTAINS
NUMEROUS PAGES
WITH THE ORIGINAL
PRINTING BEING
SKEWED
DIFFERENTLY FROM
THE TOP OF THE
PAGE TO THE
BOTTOM.

THIS IS AS RECEIVED
FROM THE
CUSTOMER.

TABLE OF CONTENTS

Page

LIST OF FIGURES iii

LIST OF TABLES v

1.0 INTRODUCTION 1
1.1 Objective . . . . .
1.2 Background 1

2.0 IONIZATION THEORY 5
2.1 General Considerations 5
2.1.1 The Influence of Cavity Size 5
2.2 Small Cavity Theory 9
2.2.1 Electronic Equilibrium Requirement 10
2.2.2 Bragg-Gray Theory 14
2.2.3 Laurence Theory 15
2.2.4 Spencer-Attix Theory 15
2.3 Large Cavity Theory 16
2.4 Burlin Theory 17

3.0 EXPERIMENTAL PROCEDURES 24
3.1 Introduction 24
3.2 Description of TLDs Used 26
3.3 Handling 26
3.4 TLD Identification 27
3.5 Irradiation Device 28
3.6 Source Material 29
3.7 Determination of Dose Rate 40
3.8 Annealing Procedures 44
3.9 Readout Equipment 46
3.10 Initial Setup 53
3.11 Analyzer Operation 55
3.12 Sensitivity Selection 56
3.13 Procedures for Encapsulated TLDs 59

4.0 RESULTS AND DISCUSSION 65
4.1 General Considerations 65
4.2 Development of Experimental and Theoretical Comparisons 66
4.3 Theoretical Results for ^{7}LiF and CaF_2:Mn TLDs 69
4.4 Experimental Results for ^{7}LiF and CaF_2:Mn TLDs . . . 72
4.5 Comparison of Theory and Experiment 73
4.6 Intercomparisons of KSU Results with ANL Results 75

Page

5.0 CONCLUSIONS 104

6.0 SUGGESTIONS FOR FURTHER STUDY 106

7.0 ACKNOWLEDGEMENTS 107

8.0 REFERENCES 108

APPENDIX A: Flow Chart of the Sensitivity Selection Procedure Incorporated in the SAD Code 111

APPENDIX B: Sensitivity Correction Factors for the Encapsulated ^{7}LiF and CaF_2:Mn TLDs From the Precision Subset 112

LIST OF FIGURES

Figure		Page
1	Absorbed dose distribution in cavity ($_{m}E_{C}$) and surrounding infinite, homogeneous medium ($_{m}E_{M}$) under uniform gamma irradiation (from Attix, et. al., (21)).	7
2	Absorbed dose distributions in cavity and surrounding material for different cavity sizes (from Attix, et. al., (21))	8
3	Relative importance of the three major types of gamma ray interactions (from Evans (24)).	12
4	$f(T_{\gamma})$ as a function of gamma ray energy for ^{7}LiF TLDs encased in a variety of electronic equilibrium capsules (calculated using the TERC/III code).	22
5	$f(T_{\gamma})$ as a function of gamma ray energy for CaF_2:Mn TLDs encased in a variety of electronic equilibrium capsules (calculated using the TERC/III code)	23
6	TLD irradiation device used in this study	30
7	Location of TLD irradiation device in reactor bay	31
8	Decay scheme for ^{51}Cr gamma ray source (from (32)). . . .	34
9	Decay scheme for ^{198}Au gamma ray source (from (32)). . . .	35
10	Decay scheme for ^{137}Cs gamma ray source (from (32)) . . .	36
11	Pulse height distribution of a 0.1 μCi ^{51}Cr source, (T_{γ} = 0.32010 MeV) (measured using the Ge(Li) system in the NAA Laboratory).	37
12	Pulse height distribution of ^{198}Au source (T_{γ} = 0.41180 MeV) (measured using the Ge(Li) system in the NAA Laboratory)	38
13	Dose rates in iron (rads/hr), due to a nominal 3.0 mCi ^{137}Cs source, as a function of radial distance (cm) from the source location. Also included is the variation of the gradient of the dose rate $\left\lvert\frac{dD(r)}{dr}\right\rvert$ $(\frac{\text{rads}}{\text{hr-cm}})$ with source distance.	43

Figure		Page
14	Arrangement of readout equipment during readouts.	47
15	Model 2000A Thermoluminescent Analyzer.	49
16	Temperature profile established for the heating planchet in the 2000A unit for use with the readout of ^{7}LiF TLDs . .	51
17	Signal-noise curves for the photomultiplier tube (Type 9856T) in the Model 2000-A unit (data supplied by the Harshaw Chemical Company).	52
18	Distribution of ^{7}LiF TLD readouts about the final precision subset mean (sensitivity selection procedure) . .	60
19	Distribution of CaF_2:Mn TLD readouts about the final precision subset mean (sensitivity selection procedure) . .	61

LIST OF TABLES

Table		Page
1	Electron Ranges in Various Sleeve Materials and Sleeve Thicknesses Used.	13
2	Gamma-ray Sources Used in the Experimental Investigation.	33
3	Location of Source Materials and Irradiation Times in the Reactor for the Production of Nominal 3.0 mCi Amounts of ^{51}Cr and ^{198}Au Isotopes (Reactor Operation: 225 kW).	39
4	Typical ^{7}LiF and CaF_2:Mn TLD Responses for an Absorbed Dose of 0.5 rad in ^{7}LiF (3.0 mCi ^{137}Cs source). . .	41
5	Irradiation Times for Bare and Encapsulated TLDs Irradiated by Nominal 3.0 mCi ^{137}Cs, ^{198}Au, and ^{51}Cr Gamma Ray Sources	45
6	Readout Cycles Used for the Analysis of ^{7}LiF and CaF_2:Mn TLDs	57
7	Encasement Materials Used During Measurement of the Energy Response of Encased ^{7}LiF and CaF_2:Mn TLDs	63
8	Partial Compilation of Input Parameter Used to Calculate the Dose Ratio $f(T_\gamma)$ Using TERC/III for 1x1x6 mm ^{7}LiF and CaF_2:Mn TLDs	77
9	Partial Compilation of Input Parmaters Used to Calculate the Dose Ratio $f(T_\gamma)$ using TERC/III for each encasement Material	78
10	$_{m}E^{calc}_{D(M)}$ Values for ^{137}Cs Source (T_γ = 0.662 MeV) and ^{7}LiF TLDs for all sleeve materials	79
11	$_{m}E^{calc}_{D(M)}$ values for ^{198}Au source (T_γ = .4118 MeV) and ^{7}LiF TLDs for all sleeve materials	80
12	$_{m}E^{calc}_{D(M)}$ values for ^{51}Cr source (T_γ = 0.320 MeV) and ^{7}LiF TLDs for all sleeve materials	81

Table | Page

13 $_{m}E^{calc}_{D(M)}$ values for ^{137}Cs source (T_γ = 0.662 MeV) and CaF_2:Mn TLDs for all sleeve materials. 82

14 $_{m}E^{calc}_{D(M)}$ values for ^{198}Au source (T_γ = 0.4118 MeV) and CaF_2:Mn TLDs for all sleeve materials. 83

15 $_{m}E^{calc}_{D(M)}$ values for ^{51}Cr source (T_γ = 0.320 MeV) and CaF_2:Mn TLDs for all sleeve materials. 84

16 Variation of $f(T_\gamma)$ with gamma-ray energy for encapsulated ^{7}LiF TLDs (from TERC/III code). 85

17 Variation of $f(T_\gamma)$ with gamma-ray energy for encapsulated CaF_2Mn TLDs 86

18 ^{7}LiF TLD readouts for various sleeve encapsulations and a ^{137}Cs gamma ray source (T_γ = 0.662 MeV) 87

19 ^{7}LiF readouts for various sleeve encapsulations and ^{198}Au gamma ray source (T_γ = 0.4118 MeV). 88

20 ^{7}LiF readouts for various sleeve encapsulations and a ^{51}Cr gamma ray source (T_γ = 0.320 MeV). 89

21 CaF_2:Mn readouts for various sleeve encapsulations and ^{137}Cs gamma-ray source (T_γ = 0.662 MeV) 90

22 CaF_2:Mn readouts for various sleeve encapsulations and ^{198}Au gamma ray source (T_γ = 0.4118 MeV). 91

23 CaF_2:Mn TLD readouts for all sleeve encapsulation materials and ^{51}Cr gamma ray source (T_γ = 0.3201 MeV). 92

24 Comparison of theory with experiment for encapsulated ^{7}LiF TLDs exposed to a nominal 3 mCi ^{137}Cs source (T_γ = 0.662 MeV). Data normalized to aluminum. 93

25 Comparison of theory with experiment for encapsulated ^{7}LiF TLDs exposed to a nominal 3 mCi ^{198}Au source (T_γ = 0.4118 MeV). Data normalized to aluminum 94

Table		Page
26	Comparison of theory with experiment for encapsulated ^{7}LiF TLDs exposed to a nominal 3 mCi ^{51}Cr source (T_γ = 0.320). Data normalized to aluminum.	95
27	Comparison of theory with experiment for encapsulated CaF_2:Mn TLDs exposed to a nominal 3 mCi ^{137}Cs source (T_γ = 0.662 MeV). Data normalized to aluminum.	96
28	Comparison of theory with experiment for encapsulated CaF_2:Mn TLDs exposed to a nominal 3 mCi ^{198}Au source (T_γ = 0.4118 MeV). Data normalized to Al	97
29	Comparison of theory with experiment for encapsulated CaF_2:Mn TLDs exposed to a nominal 3 mCi ^{51}Cr source. (T_γ = 0.320 MeV). Data normalized to Al.	98
30	Comparison of theory with experiment for encapsulated ^{7}LiF TLDs exposed to a nominal 3 mCi ^{137}Cs source (T_γ = 0.662 MeV). Data normalized to stainless steel	99
31	Comparison of theory with experiment for encapsulated ^{7}LiF TLDs exposed to a nominal 10 mCi ^{137}Cs source (data taken at Argonne National Laboratory, normalized to stainless steel).	100
32	Comparison of theory with experiment for encapsulated CaF_2:Mn TLDs exposed to a nominal 10 mCi ^{137}Cs source (data taken at Argonne National Laboratory, May 1977, normalized to aluminum)	101
33	Intercomparison of C/E ratios of KSU data and ANL data for ^{137}Cs source and ^{7}LiF TLDs. (Data referenced to stainless steel).	102
34	Intercomparison of C/E ratios of KSU data and ANL data for ^{137}Cs source and CaF_2:Mn TLDs. (Data referenced to aluminum).	103

1.0 INTRODUCTION

1.1 Objective

The overall objective of this research was to investigate the use of encapsulated thermoluminescent dosimeters (TLDs) to measure gamma ray energy deposition in lead, tantalum, tin, copper, stainless steel, iron, and aluminum. In particular, it was desired to verify theoretical calculations of energy deposition in these materials with experimental results for low values of gamma energies (0.3-0.7 MeV).

An important sub-objective of this research was to develop a suitable dosimetry system (consisting of an irradiation device, encapsulated and preferably monoenergetic gamma-ray sources, and properly calibrated readout equipment) so as to minimize experimental error whenever possible.

1.2 Background

From a theoretical viewpoint, encapsulated TLDs are treated as a special case of the more general situation of a medium containing a cavity. The cavity consists of a radiation-sensitive device that may be either solid, liquid, or gaseous, and is usually of a different atomic number and density than the surrounding medium (though this need not necessarily be the case). The radiation-sensitive device is usually termed a "dosimeter", if it is used to measure the absorbed dose due to radiation in the surrounding medium. In order to

meaningfully evaluate the dosimeter response, one must know the ratio of the energy absorbed in the dosimeter to that of the surrounding material (known as the f ratio). For the same type dosimeter used, this ratio is a function of the atomic number of the surrounding material, the size of the dosimeter, and the energy of the incident radiation.

The first rigorous statement of cavity ionization theory is due to Gray (1,2) in which he stated his "principle of equivalence". This principle was based on the assumption that the introduction of a gas-filled cavity into a medium did not perturb the flow of the electron spectrum in the medium surrounding the cavity. He proved this to be true for small cavities, (i.e., small compared to the ranges of the primary electrons in the surrounding medium). The Bragg-Gray relation, derived in 1936, assumed that the energy lost by electrons traversing both solid and gaseous volume elements was equal to the energy absorbed within that volume, i.e., continuous energy loss. He proved that the ratio of the energy absorbed per unit volume of solid to that of the gas was equal to the ratio of the electron stopping powers of the solid and gas. He also stated that this ratio (termed $_{m}s$) was "almost independent" of the energy of the electrons.

In 1937, Laurence (3) took into account the energy dependence of the stopping power by averaging the $_{m}s$ values over the total

spectrum of electrons traversing the cavity to obtain a mean value of $_{m}s$. Both Gray and Laurence, however, neglected to take into account the production of fast secondary electrons (δ-rays) produced by electron-electron collisions that leave the cavity thus making the continuous energy loss assumption invalid.

Spencer and Attix (4) and Burch (5) took secondary electron effects into account in developing the theory. This provided a better approximation to $_{m}s$ (6) than did the theories of Gray and Laurence. However, all theories developed thus far did not consider the perturbation effects of the cavity on the primary electron spectrum generated in the wall material and therefore could not be used to describe the situation for intermediate and large sized cavities.

In 1953, Daniels, et al., (7) suggested the use of TLDs in radiation dosimetry. Since TLDs fall into the "intermediate sized cavity" category, the theory had not been adequately developed to predict absorbed dose for various encapsulation materials. In 1966 Burlin (8) developed a "general theory of cavity ionization" which took the size effect of the cavity into account, and could be applied to small, intermediate and large sized cavities.

Experimental verifications of the theories of Bragg-Gray and Spencer-Attix were carried out by Burlin (9-14). Verifications of the "general theory of cavity ionization" for Fricke dosimeters were carried out by Burlin and Chan (15).

Lithium fluoride powder TLD material containing enriched ^{7}Li (99.997%) was used by Adamson, et al. (17) to measure the fine structure within a single cell at the center of ZEBRA-6. Simons (18) reported gamma-ray dose measurements using 1x1x6 mm solid entruded TLD rods encased in stainless steel for ZPR-3 Assembly 60 at Argonne National Laboratory. Results from all these investigations showed that it was feasible to use TLDs inside critical assemblies.

Simons and Yule (19) reported calculations using the "general cavity ionization theory" of Burlin and experimental data to support the theory. Experiments were performed at the ZPPR-2 in support of the design of the LMFBR Demonstration Reactor at Argonne National Laboratory. ^{7}LiF TLDs encapsulated with a variety of electron-equilibrium sleeves were used and the results were compared with the theoretical calculations (20).

2.0 IONIZATION THEORY

2.1 General Considerations

In Chapter 1 it was stated that the size of the cavity played an important role in determining the f ratio for solid-state cavities. A small cavity is defined as one in which the linear dimensions are small compared to the ranges of the primary electrons generated in the surrounding wall material. The cavity thus defined does not perturb the primary electron flux generated in the wall material. The theories of Bragg-Gray (2), Laurence (3), and Spencer-Attix (4) are admirably suited for this situation. In the case of TLDs, however, the size of the cavity is now large enough to perturb the flux, and Burlin's theory (8) must be used to determine the f ratio. Before discussing the details of the various theories, it is necessary to qualitatively discuss the influence of the cavity size on the relative absorbed doses in the cavity and wall material.

2.1.1 The Influence of Cavity Size

Consider a cavity embedded in a homogeneous medium. The cavity may be either solid, liquid, or gaseous in nature. The surrounding medium may contain a uniformly distributed radioactive source, or be subjected to a uniform beam of radiation. In the case of a uniform homogeneous medium only, the absorbed dose per unit mass, ${}_{m}E_{M}$, for a gamma ray source, would be the energy lost per unit mass of all gamma

rays present. For a monoenergetic gamma ray source of energy T_γ, the absorbed dose will be

$$ {}_mE_M = N\, T_\gamma \left(\frac{\mu_{en}}{\rho}\right)_M \qquad (2.1) $$

where

N = fluence of gamma rays of energy T_γ (gammas/cm^2)

$\left(\frac{\mu_{en}}{\rho}\right)_M$ = mass energy absorption coefficient of medium for gamma rays of energy T_γ (cm^2/g).

Consider the introduction of a radiation-sensitive cavity of different material into the homogeneous medium. Figure 1 illustrates the variation of the absorbed dose distribution in the presence of the cavity. Using the subscripts M and C to denote material and cavity, respectively, it is here assumed that ${}_mE_M > {}_mE_C$. At a large distance from the cavity boundary, the absorbed dose reaches a constant value in each material. The magnitude of this value equals the absorbed dose in an infinite medium composed of that material. At regions near the cavity boundary, the absorbed dose distribution is dependent on the properties of the two materials. At the cavity boundary itself, there is a discontinuity in the absorbed dose distribution due to the difference in the stopping powers of the electrons traversing the two media (21).

Now consider the variation in size of the cavity. Referring to Fig. 2(a), for a large cavity, the dimensions are much larger than the ranges of the electrons and the absorbed doses in the cavity and in the surrounding material are the constant-value infinite-medium

THIS BOOK CONTAINS NUMEROUS PAGES WITH DIAGRAMS THAT ARE CROOKED COMPARED TO THE REST OF THE INFORMATION ON THE PAGE.

THIS IS AS RECEIVED FROM CUSTOMER.

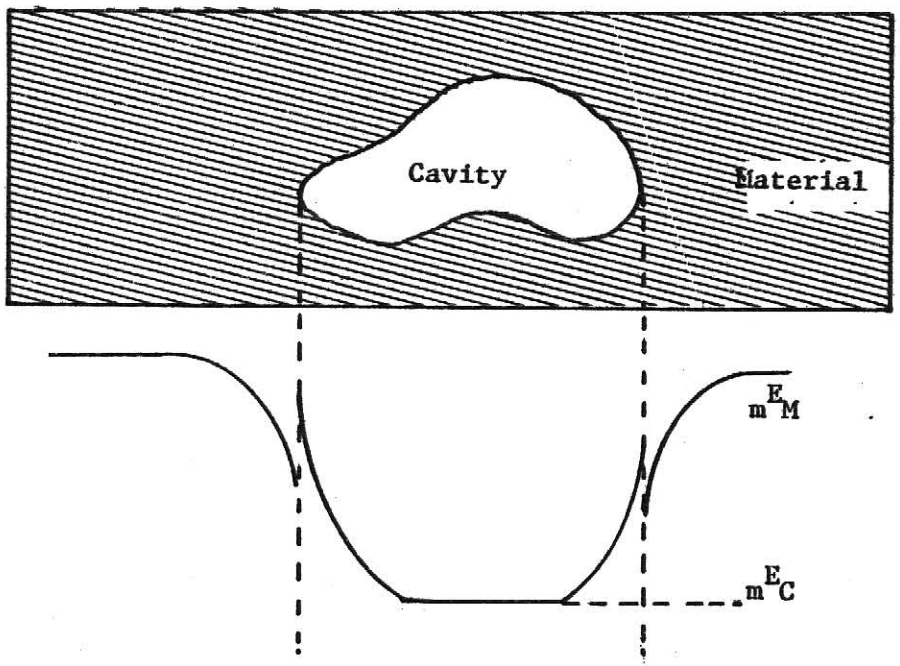

Fig. 1. Absorbed dose distribution in cavity ($_mE_C$) and surrounding infinite, homogeneous medium ($_mE_M$) under uniform gamma irradiation (from Attix, et al., (21)).

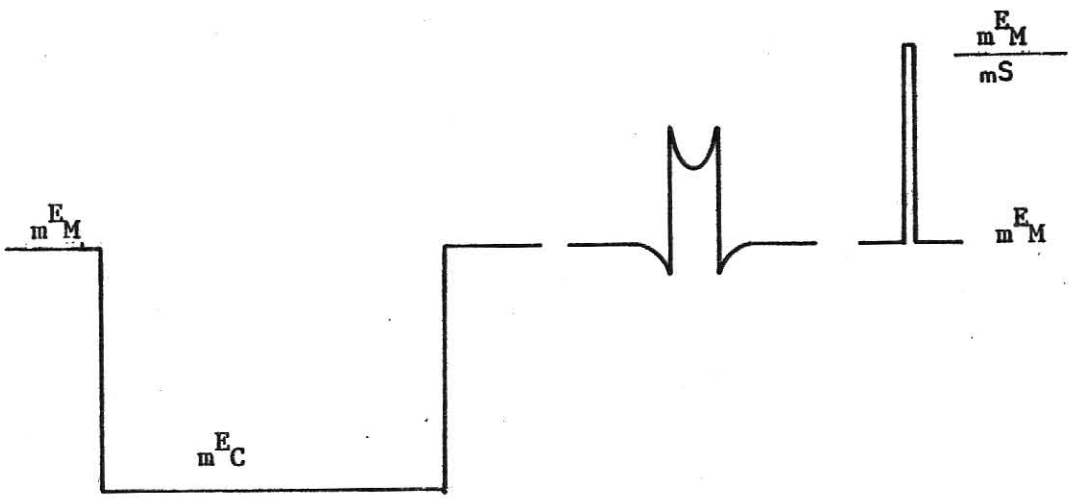

(a) LARGE CAVITY (b) INTERMEDIATE CAVITY (c) SMALL CAVITY

Fig. 2. Absorbed dose distributions in cavity and surrounding material for different cavity sizes (from Attix, et al., (21)).

absorbed doses. The contribution to the absorbed dose in the interface region is negligible. Referring to Fig. 2(c), for a small cavity, the cavity size is not sufficient to perturb the primary electron flux generated in the surrounding material. Consequently, the absorbed dose in the cavity is simply that in the surrounding medium divided by the ratio of the mass stopping powers of the electrons in the cavity and the surrounding material, ${}_{m}s$. In this case, ${}_{m}s$ is assumed less than 1; this need not be the case in general. Referring to Fig. 2(b), for an intermediate sized cavity, the cavity size is large enough to perturb the primary electron flux. The degree of perturbation is a function of

(1) The ratio of the cavity diameter to the primary electron range.

(2) The ratio ${}_{m}E_{M}/{}_{m}E_{C}$.

2.2. Small Cavity Theory

All small cavity theories discussed here are based on the following assumptions:

(1) The electron spectrum established in the medium surrounding the cavity is not modified by the presence of the cavity.

(2) Photon interactions generating electrons in the cavity are negligible.

(3) The small cavity is surrounded by a material under uniform irradiation.

(4) Electronic equilibrium exists uniformly within the material.

Requirements (1) through (3) above are self-explanatory. Requirement (4) is valid for any sized cavity, and needs to be explained in more detail.

2.2.1 Electronic Equilibrium Requirement

There are two types of electronic equilibrium, complete and transient (6). The former is said to exist at a point when, for every electron leaving a volume element surrounding the point, another of the same energy enters to take its place. This condition exists only in the case of a uniformly distributed radioactive emitter in a large medium, and only at points far removed from the boundary. When a beam of gamma rays enter the medium, however, at a certain depth into the medium, the ratio of the energy absorbed to that released within a volume element reaches a constant value, independent of position. This is known as transient equilibrium. A certain minimum sleeve thickness is required in order to satisfy this requirement. If possible, the sleeve thickness should be equal to the range of the most energetic electron produced in the wall (22). However, it has been pointed out by Boag (23) that a sleeve thickness smaller than the maximum electron range may be sufficient to ensure electronic equilibrium.

Evaluation of the maximum electron energy in the sleeve depends on the sleeve material and the maximum incident gamma ray energy. If the photoelectric effect is dominant, then the maximum electron energy is set equal to the gamma ray energy. If Compton scattering is dominant, then the maximum electron energy, T_{max}, for gamma rays of energy T_γ is given by

$$T_{max} = \frac{T_\gamma}{1 + (\alpha/2)} \qquad (2.2.)$$

where

$$\alpha = \frac{T_\gamma}{m_o c^2}$$

and

$m_o c^2$ = 0.511 MeV, the electron rest energy.

For the pair production reaction, the gamma ray is entirely absorbed and produces a positron-negatron pair of energies E_+ and E_-, respectively, where

$$T_\gamma = E_+ + E_- \; 2m_o c^2 \qquad (2.3)$$

In the energy range under investigation (0.3 - 0.7 MeV) the following sources were used for TLD irradiation: ^{137}Cs (T_γ = 0.662 MeV), ^{198}Au (T_γ = 0.41180 MeV) and ^{51}Cr (T_γ = 0.32010 MeV). For the ^{137}Cs source, the Compton effect is dominant in all sleeve materials. For the ^{198}Au and the ^{51}Cr source, the Compton effect is dominant in all sleeve materials except for lead and tantalum, where the photoelectric effect is dominant. This can be verified with reference to Fig. 3.

It is useful to compare the electron range in the various sleeve materials with the actual thickness of the sleeves used. This comparison is made in Table 1. In most cases, the sleeve thickness was as great as the range of the most energetic electron.

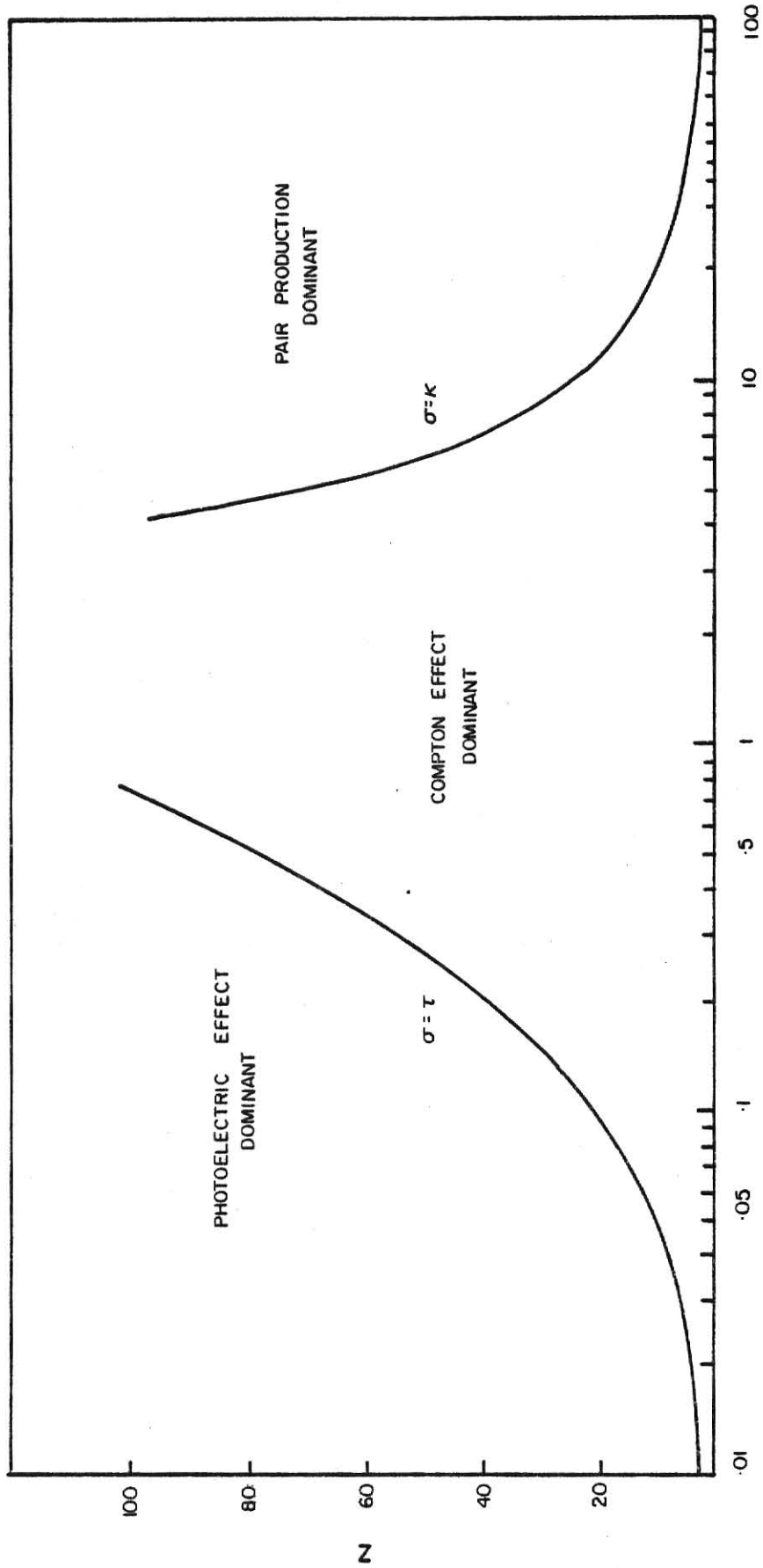

Fig. 3. Relative importance of the three major types of gamma ray interactions (from Evans (24)).

Table 1. Electron Ranges in Various Sleeve Materials and Sleeve Thicknesses Used.

Electron Energy (MeV)	Range (g/cm^2)	Ranges in Various Sleeve Materials (cm)						
		S.S.	Fe	Al	T_a	S_n	Pb	Cu
0.1	0.0135	0.0017	0.0017	0.0050	0.0008	0.0018	0.0012	0.0015
0.2	0.0420	0.0054	0.0053	0.0156	0.0025	0.0058	0.0037	0.0047
0.3	0.0782	0.0100	0.0099	0.0290	0.0047	0.0107	0.0069	0.0087
0.4	0.1193	0.0153	0.0152	0.0442	0.0072	0.0163	0.0150	0.0133
0.5	0.1638	0.0210	0.0208	0.0607	0.0098	0.0224	0.0144	0.0183
0.6	0.2106	0.0270	0.0268	0.0780	0.0127	0.0288	0.0186	0.0235
0.7	0.2592	0.0332	0.0329	0.0960	0.0156	0.0355	0.0229	0.0289
1.0	0.4120	0.0524	0.0524	0.1526	0.0248	0.0564	0.0363	0.0460
Sleeve Thickness (cm)	-	0.0889	0.0833	0.1905	0.0419	0.0833	0.0648	0.0775

2.2.2 Bragg-Gray Theory

Consider two volume elements, one consisting of a gas-filled cavity and the other a solid volume element of the surrounding material under uniform radiation. Assume that the respective linear dimensions of the two volume elements are in the ratio s:1, where s is the ratio of the electron stopping powers of the solid to that of the gas. Then Gray's "principle of equivalence" (21) states that, "The energy lost per unit volume by electrons in the cavity is 1/s times the energy lost by gamma rays per unit volume of the solid."

Going from the "principle of equivalence" to the Bragg-Gray theory, Gray made the crucial assumption that the energy lost by electrons in traversing the two volume elements is equal to the energy absorbed within that particular element. Thus, if ${}_vE$ is the energy absorbed per unit volume of solid, and ${}_vJ$ is the ionization per unit volume of gas,

$$ {}_vE = s\, W\, {}_vJ \qquad (2.4) $$

where

W = average energy required for the formation of one ion pair in the gas (assumed constant and independent of electron energy).

In developing the Bragg-Gray theory, Gray also made the important assumption that the ratio of stopping powers of the solid to that of the gas, s, was independent of the electron energy. In a later development, Laurence (25) took the energy dependence of the electron stopping power ratio into account.

2.2.3 Laurence Theory

The Bragg-Gray equation can be rewritten in terms of unit mass as

$$m^s = \frac{m^E}{W_m J} \tag{2.5}$$

Laurence took the energy dependence of $_m s$ into account by spectrum-averaging $_m s$ over the equilibrium spectrum of electrons slowing down with initial energy T_o. Thus he derived that

$$\frac{1}{\overline{m^s}} = \int_o^{T_o} \frac{dT}{m^s} . \tag{2.6}$$

Further spectrum-averaging can be carried out in cases where there is a spectrum of initial starting energies $A(T_\gamma, T_o)$ for mono-energetic gamma rays of energy T_γ, in which case,

$$\frac{1}{\overline{m^s}} = \frac{\int_o^{T_{max}} A(T_\gamma, T_o)\ T_o\ (dT_o / \overline{m^s})}{\int_o^{T_{max}} A(T_\gamma, T_o)\ T_o\ dT_o} \tag{2.7}$$

where T_{max} is the max electron energy in the initial electron spectrum. Here again the continuous-loss assumption of Gray is valid and it has been assumed that energy lost by electrons equals the energy absorbed (no delta-ray production). The NCRP (6) has expressed equations (2.7) and (2.8) in more convenient algebraic forms.

2.2.4 Spencer-Attix Theory

Both the Bragg-Gray and Laurence theories assumed continuous energy loss of the primary electrons in both cavity and wall material. They neglected to take into account fast secondaries produced by primary

knock-on collisions (delta rays) that leave the region of interaction and consequently do not deposit their energy at the point of interaction. Spencer and Attix attempted to take secondaries into consideration by defining an energy threshold Δ, below which the secondaries were assumed to deposit their energy at the point of interaction.

An important conclusion from Spencer-Attix theory is that the stopping power ratio $\overline{s}_m$ is cavity size dependent. The reasoning is as follows. For primary gamma-ray interactions within the cavity, energy transfers of less than Δ arising from primary electron knock-on collisions are deposited in the cavity. Energy transfers greater than Δ are carried out of the cavity. Consequently, Δ is a measure of the size of the cavity, and is in fact the energy of the secondary electron that will just cross the cavity.

2.3 Large-Cavity Theory

In cases where the cavity size is very much larger than the range of the primary electrons, it has been shown in Section 2.1 that the energy absorbed in the cavity is a function of the properties of the cavity. Similarly, the energy absorbed in the surrounding material is a function of the properties of the material. For a gamma-ray source, the energy absorbed is a function of the mass-energy absorption coefficient in either case. Hence, the energy absorbed in the medium per unit mass, $_mE_M$, can be related to the energy absorbed per unit mass in the cavity, $_mE_C$, by the relation

$$ {}_{m}E_{M} = \frac{(\mu_{en}/\rho)_{M}}{(\mu_{en}/\rho)_{C}} \, {}_{m}E_{C} \qquad (2.8) $$

2.4 Burlin Theory

The theories of Bragg-Gray, Laurence and Spencer-Attix are all based on the assumption that the introduction of a small gas-filled cavity into a medium under uniform irradiation does not perturb the primary electron spectrum established in the wall material. As the cavity size is increased, however, flux perturbation effects become significant. This fact was verified by the NCRP (6) using results obtained by Attix et al. (26) for a parallel plate ionization chamber, where the spacing between the plates was varied from 0.5-10 mm. For a cavity filled with air at 1 atm pressure, in a medium irradiated with gamma rays of energy exceeding 1 MeV, small cavity theory would apply if the linear dimensions of the cavity were 1 cm or less (21). Solid cavities are about 1000 times as dense as air, and for small cavity theory to apply, the linear dimensions must be of the order of 10^{-3} cm or less, which is clearly unrealistic. In order to develop a theory suitable for solid and liquid cavities also, Burlin (8) sought to remove the size restriction inherent in small cavity theory by taking into account the flux perturbation effect as the cavity size is increased to intermediate size. This flux perturbation effect is twofold:

(i) It accounts for an exponential attenuation, in the cavity, of the primary electrons generated by photon interactions in the medium. The shape of the spectrum remains unchanged (21).

(ii) It accounts for a buildup of the primary electrons generated in the cavity due to photon interactions in the cavity.

For a monoenergetic gamma ray source of energy T_γ, Burlin's development can be written as

$$f(T_\gamma) = F_M(T_\gamma)\ f_s(T_\gamma) + F_D(T_\gamma)\ f_\ell(T_\gamma) \qquad (2.9)$$

where

$f_s(T_\gamma)$ = f ratio assuming small cavity theory

$f_\ell(T_\gamma)$ = f ratio assuming large cavity theory

$F_M(T_\gamma)$ = primary electron attenuation factor in the cavity (as per (i) above)

$F_D(T_\gamma)$ = buildup factor for primary electrons generated in cavity (as per (ii) above).

Here $F_M(T_\gamma)$ approaches unity for small cavities or high gamma ray energies, and zero for large cavities or low gamma-ray energies. The exactly reverse logic applies to $F_D(T_\gamma)$. $F_M(T_\gamma)$ is thus a function of the mean chord length, g, of the dosimeter, defined by

$$g = \frac{4V\rho}{S}\ (g/cm^2) \qquad (2.10)$$

where V is the volume, ρ the density and S the surface area of the dosimeter. If $\beta(T_\gamma)$ is the attenuation coefficient for gamma rays of energy T_γ,

$$F_M(T_\gamma) = \int_o^g e^{-\beta(T_\gamma)\, x}\, dx \Big/ \int_o^g dx$$

$$= \frac{1 - \exp\left[-\beta(T_\gamma)g\right]}{\beta(T_\gamma)g} \qquad (2.11)$$

and

$$F_D\ (T_\gamma) = 1 - F_M(T_\gamma) \qquad (2.12)$$

The Katz and Penfold expression (27) was used for $\beta(T_\gamma)$, given by

$$\beta\ \ (T_\gamma) = -\frac{\ln 0.01}{R(T_\gamma)} \qquad (2.13)$$

where $R(T_\gamma)$ is the range of primary electrons of maximum energy T_γ given by

$$R(T_\gamma) = \begin{cases} 0.412\ T_\gamma^n & \text{for } 0.01 \leq T_\gamma \leq 3 \text{ MeV} \\ 0.530\ T_\gamma - 0.106 & \text{for } 3.0 < T_\gamma \leq 20 \text{ MeV} \end{cases} \qquad (2.14)$$

and

$$n = 1.265 - 0.0954 \ln T_\gamma\ . \qquad (2.15)$$

The Laurence theory is used in calculating $f_s(T_\gamma)$ in Eq. (2.9) for solid filled cavities (28) for the following reason. The difference between the discrete energy loss stopping power ratio (Spencer-Attix theory) and the spectrum averaged continuous energy loss stopping power ratio for electrons (Laurence) is less than a few percent for $\Delta > 100$ keV (29). The parameter Δ used here is a discrete energy loss parameter that represents the maximum kinetic energy of the secondary electron that just crosses the cavity. For

1x1x6 mm TLDs, with an average chord length of 0.27 g/cm^2, Δ corresponds to 436 keV. Since this is significantly larger than 100 keV, secondary electron effects can be ignored and the continuous energy-loss assumption is adequate.

In Section 2.2.2, the reciprocal of the stopping power ratio, $\frac{1}{\frac{}{s}}$, which is equal to the f ratio, $f_s(T_\gamma)$, was derived for an initial electron energy T_o as

$$\frac{1}{\frac{}{s}} = f_s(T_\gamma) = \frac{1}{T_o}\int_o^{T_o} \frac{1}{\frac{}{s}}\, dT$$

$$= \frac{1}{T_o}\int_o^{T_o} \frac{S_{coll_D}(T)}{S_{coll_M}(T)}\, dT \qquad (2.16)$$

where $S_{coll}(T)$ is the mass stopping power of electrons of energy T. In the case where there is a spectrum of starting energies $N_m(T_\gamma,T_o)$ defined by:

$N_M(T_\gamma,T_o)dT$ = fraction of photon energy transferred to initial electron with energy in the interval (T_o,dT_o)

the stopping power ratio must be further averaged over this spectrum of starting energies. Thus we have

$$f_s(T_\gamma) = \int_o^{T_\gamma} N_M(T_\gamma,T_o)dT_o \left\{\frac{1}{T_o}\int_o^{T_o} \frac{S_{coll_D}(T)}{S_{coll_M}(T)}\, dT\right\} \qquad (2.17)$$

From the section on large cavity theory, we can write

$$f_1(T_\gamma) = \frac{\left[\frac{\mu_{en}(T_\gamma)}{\rho}\right]_D}{\left[\frac{\mu_{en}(T_\gamma)}{\rho}\right]_M} \tag{2.18}$$

and the general ratio $f(T_\gamma)$ can be written as

$$f(T_\gamma) = F_M(T_\gamma) \int_o^T N_M(T_\gamma, T_o)\, dT_o \left[\frac{1}{T_o} \int_o^{T_o} \frac{S_{coll_D}(T)}{S_{coll_M}(T)}\, dT\right] +$$

$$+ F_D(T_\gamma) \frac{\left[\frac{\mu_{en}(T_\gamma)}{\rho}\right]_D}{\left[\frac{\mu_{en}(T_\gamma)}{\rho}\right]_M} \tag{2.19}$$

A computer code TERC/III written by Simons (private communication) calculates $f(T_\gamma)$ for a variety of encasement materials. Figures 4 and 5 illustrate $f(T_\gamma)$ as a function of gamma-ray energy for 1x1x6 mm ^7LiF and CaF_2:Mn TLDs encased in electronic equilibrium sleeves.

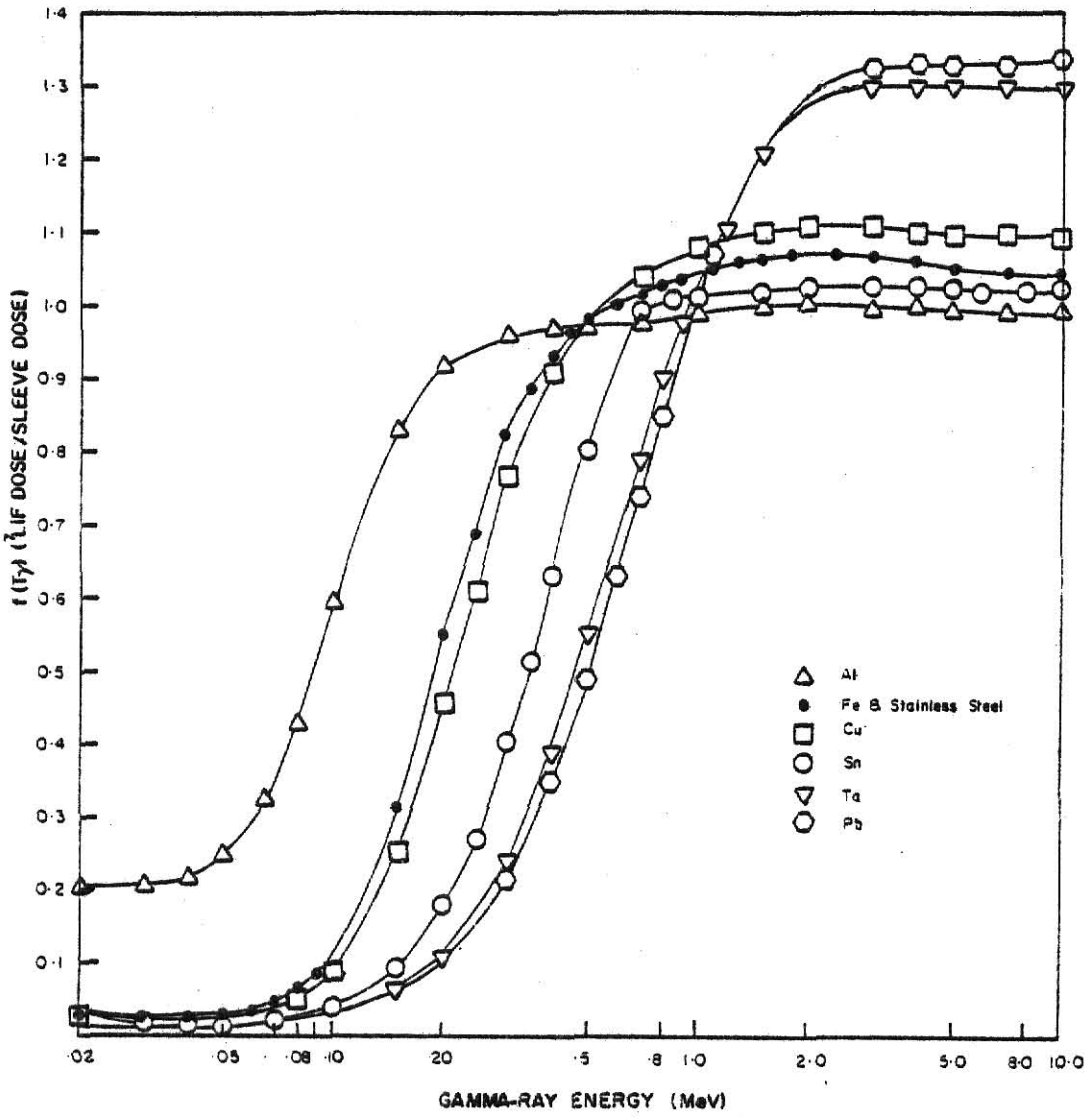

Fig. 4. $f(T_\gamma)$ as a function of gamma-ray energy for ^{7}LiF TLDs encased in a variety of electronic equilibrium capsules (calculated using the TERC/III code).

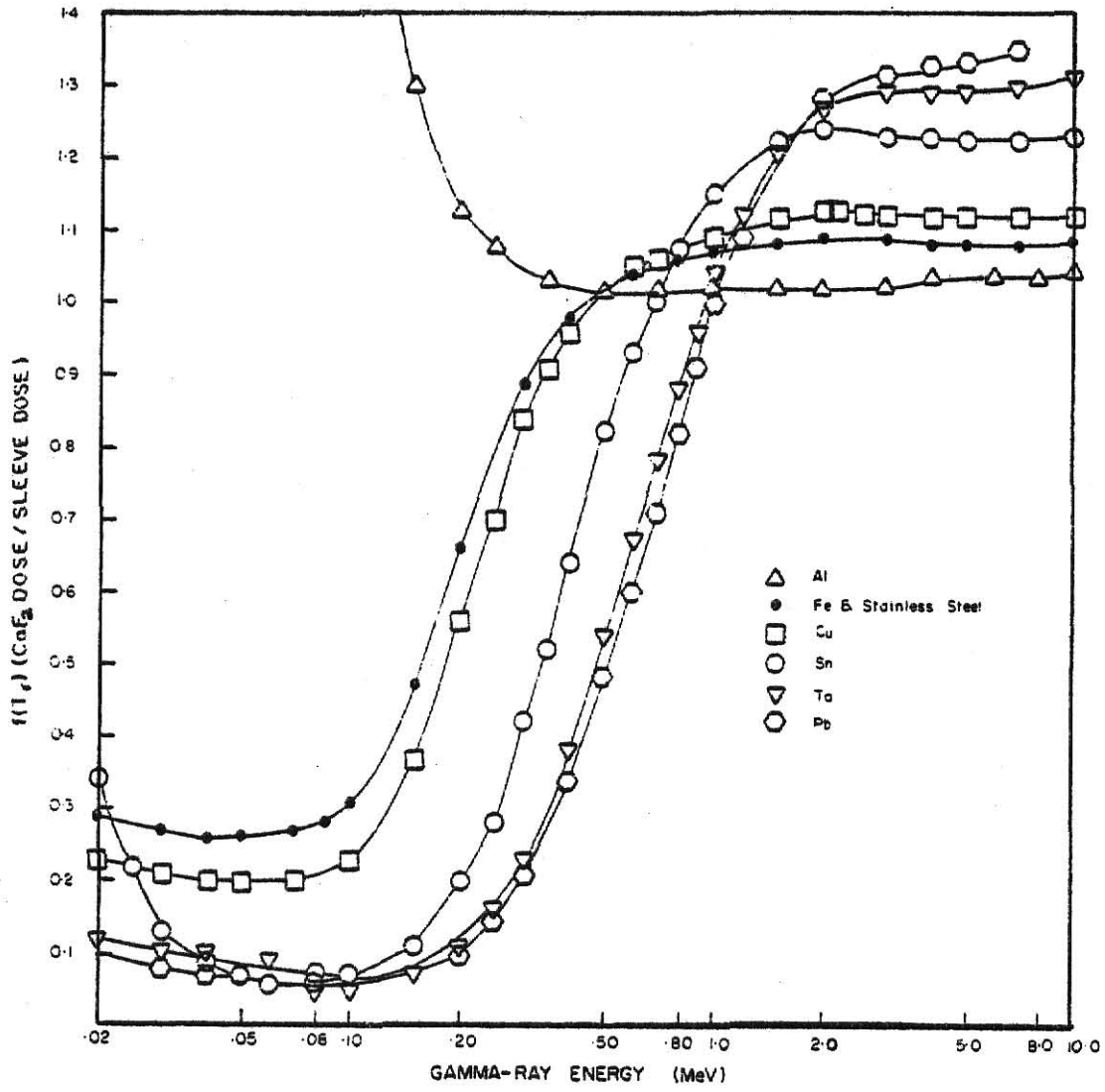

Fig. 5. $f(T_\gamma)$ as a function of gamma-ray energy for CaF_2:Mn TLDs encased in a variety of electronic equilibrium capsules (calculated using the TERC/III code).

3.0 EXPERIMENTAL PROCEDURES

3.1 Introduction

Experimental procedures used in obtaining the thermoluminescent output (response) of encapsulated 1 x 1 x 6 mm ^{7}LiF and CaF_2:Mn TLDs will be discussed in this chapter. Encapsulation materials (sleeves) selected for this research project were: iron, tantalum, lead, stainless steel, copper, tin, and aluminum. Gamma-ray sources used for TLD irradiation were: ^{137}Cs (T_γ = 0.662 MeV), ^{198}Au (T_γ = 0.4118 MeV) and ^{51}Cr (T_γ = 0.3201 MeV). Briefly, the following procedure was established for each type of TLD and gamma-ray source. A precision subset was selected from a batch of approximately 220 TLDs through sensitivity selection. The precision subset was further subdivided into groups of 15-20 TLDs, and following annealing, individual TLDs from each group were encapsulated with one type of sleeve material. After irradiation of the encapsulated TLDs, the thermoluminescence (TL) was measured using the readout procedure described in Section 3.11. Normalized experimental and calculated responses were then compared as a function of gamma-ray energy, sleeve material and TLD type, as discussed in Chapter 4.

Obtaining TLD responses with good precision was complicated by the fact that the TL emitted was highly sensitive to the handling, irradiation, annealing and readout procedures used. Well established and reliable procedures have been developed at Argonne National

Laboratory for the use and handling of TLDs. These procedures were carefully adhered to at all times.

This chapter is organized in the following manner. Section 3.2 describes the ^{7}LiF and CaF_2:Mn TLDs used in the investigation. Section 3.3 presents the procedures used in the care and handling of TLDs. The methods used for the identification of bare and encapsulated TLDs during the experimental procedure are clarified in detail in Section 3.4. Bare and encapsulated TLDs were supported on an irradiation device during irradiation by a gamma-ray source. The considerations involved in the design of such a device and the actual device used for the experiments are discussed in Section 3.5. Section 3.6 presents the considerations involved in the selection of source materials used to produce the isotopes required for this investigation. The selection of the radial location of the TLDs from the source location, from dose-rate considerations, is discussed in Section 3.7. The annealing procedures used for the TLDs, before and after irradiation by a gamma-ray source, are described in Section 3.8. The readout equipment used for analyzing TLDs is described in Section 3.9. Prior to analyzing TLDs, a systematic procedure was used for initial setup of equipment. This initial setup procedure is described in Section 3.10. The procedure used to obtain the TLD response, subsequent to initial setup of equipment, is described in Section 3.11. Precision subsets were selected

from the original batch of ^{7}LiF and CaF_2:Mn TLDs used for this investigation. This selection procedure, known as sensitivity selection, is described in Section 3.12. Lastly, the types of sleeve materials used and the procedures for encapsulated TLDs are described in detail in Section 3.13.

3.2 Description of TLDs Used

^{7}LiF and CaF_2:Mn TLDs were used in this study. The ^{7}LiF TLDs were of high sensitivity type, in the form of 1 x 1 x 6 mm rods, manufactured from TLD-700[1] (which consists of 99.931% ^{7}Li and 0.07% ^{6}Li). The CaF_2:Mn TLDs were in the form of 1 x 1 x 6 mm rods and manufactured from TLD-400. Both types of TLDs were supplied by the Harshaw Chemical Company.

3.3 Handling

Improper handling of TLDs can have a significant detrimental effect on the reproducibility of their responses. The term "handling" here refers to the manner in which individual TLDs are supported and the measures used to protect the TLDs from ambient light.

The thermoluminescent output of a TLD is altered if touched by bare hands (surface contamination), or dropped on a hard surface. In addition, scratching of the crystal surface also alters the TLD response. Consequently, bare TLDs were always carried by plastic-tipped tweezers, and supported on several layers of tissue between readouts.

[1] Contains Mg and Ti activators, commonly designated as ^{7}LiF:Mg,Ti

Fading effects (i.e., a decrease in the TLD response due to exposure to ambient light) in ^{7}LiF and CaF_2:Mn TLDs have been noted by various investigators (22,30,31). Consequently, bare and encapsulated TLDs were placed in individual, opaque envelopes and stored in an enclosed cabinet after irradiation. Additional precautions were taken for CaF_2:Mn TLDs during and after irradiation. During irradiation, CaF_2:Mn TLDs were covered with black paper to minimize fading effects due to ambient light. Fluorescent lights were turned off prior to readout, and a minimal amount of incandescent lighting was used during readout. After each TLD was removed from its sleeve, prior to readout, it was covered with black paper to minimize fading due to the incandescent lighting.

3.4 TLD Identification

Bare TLDs cannot be marked for identification on the crystal surface. Therefore, other methods had to be used for identification purposes. During annealing, bare TLDs were placed in individual holes in the aluminum annealing plate. Since each hole location was numbered in sequence, it was possible to retain the identity of each TLD. During irradiation for sensitivity selection, the identity of each TLD was also retained as it was placed on the irradiation device. After irradiation, each TLD was placed in a numbered envelope. The sleeves used for TLD encapsulation were also numbered, and the same TLD-sleeve combination was maintained for all

irradiations. After irradiation, each encapsulated TLD was placed in an opaque envelope that identified the TLD, the sleeve type and number.

3.5 Irradiation Device

An irradiation device was constructed to support the bare or encapsulated TLDs and the source during irradiation. For this research it was important to irradiate the TLDs with the primary unscattered flux from the source. Hence, it was desirable to use a lightweight material that was as transparent as possible to gamma rays. Likewise, the device should be situated at a sufficient distance from walls, ceilings, floors, and other objects that may add a scattered component to the total TLD dose.

Based on these considerations, two materials were tested for use at Kansas State University: plexiglass and styrofoam. A 120 x 120 x 1.27 cm plexiglass sheet was supported horizontally on top of a vertical plastic pipe, measuring 30.5 cm in diameter and 305 cm long. To evaluate the scattering properties of this device, a ^{137}Cs source was placed at the center of the sheet, and the transmitted pulse height distribution was measured by means of a 3" x 3" NaI(Tl) scintillation detector, mounted vertically under the sheet. The primary pulse height distribution was measured, for the same source-detector configuration, with the plexiglass sheet removed. Comparison of the primary and transmitted pulse height distributions revealed a significant reduction in the peak height of the primary gamma ray

line. This indicated that plexiglass was not an acceptable material. A styrofoam sheet, measuring 120 x 120 x 2.5 cm was then suspended from the crane hook in the reactor bay at the same location at which the plexiglass sheet was tested. The primary and transmitted pulse height distributions were measured in the same manner. Within the statistical limits of the data, they were identical. Styrofoam was therefore chosen as the construction material for the irradiation device.

The final irradiation assembly (see Fig. 6) consisted of a styrofoam sheet suspended by nylon rope from the crane hook in the reactor bay. Lead bricks held the rope taut and stabilized the assembly. As shown in Fig. 7, the device was situated at a height of more than 300 cm (10 feet) from the floor and reactor walls.

Precautions were taken to ensure that TLD irradiation periods did not coincide with reactor operations. Spurious radiations present in the reactor bay during reactor operations would have introduced unwanted components to the total TLD dose.

3.6 Source Material

With the exception of ^{137}Cs (a 3.0 mCi source was available), gamma-ray sources used for TLD irradiation were produced through neutron activation in the Kansas State University Triga reactor. Consequently, a primary requirement for the source materials selected was that they have a reasonably high neutron-activation cross-section

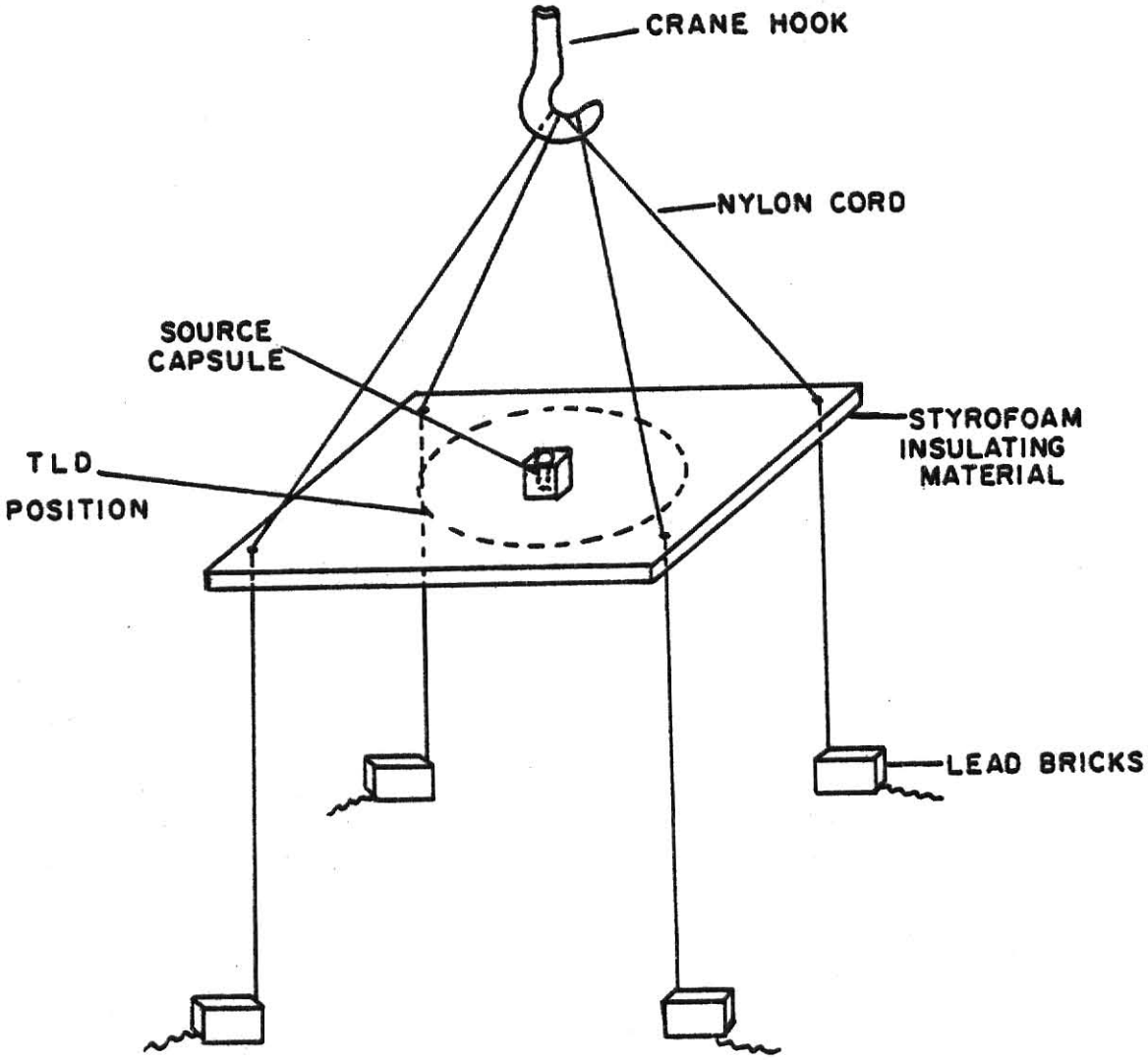

Fig. 6. TLD irradiation device used in this study.

THIS BOOK CONTAINS SEVERAL DOCUMENTS THAT ARE OF POOR QUALITY DUE TO BEING A PHOTOCOPY OF A PHOTO.

THIS IS AS RECEIVED FROM CUSTOMER.

Fig. 7. Location of TLD irradiation device in reactor bay.

for the production of the particular isotopes, and that the isotopes emitted gamma rays with the desired energies and known yields in the range 0.1-0.7 MeV. The source materials selected and isotopes produced are listed in Table 2. Decay schemes for the three isotopes selected are shown in Figs. 8, 9, and 10. Approximately 4.8 g of 99.997% pure (spectroscopic grade material) chromium and a gold foil (weighing approximately 0.1 g), were used to produce nominal 3.0 mCi amounts of ^{51}Cr and ^{198}Au, respectively. The location of the source materials in the reactor during isotope production and the irradiation times used are shown in Table 3.

Pulse height distributions were measured for the ^{198}Au and ^{51}Cr isotopes. For measurement purposes, a small quantity (.063 g) of Chromium was used to produce 0.1 μCi of ^{51}Cr during production of the 3.0 mCi ^{51}Cr isotope. The measured pulse height distribution of the 1 μCi ^{51}Cr isotope using the Ge(Li) system in the Neutron Activation Analysis (NAA) Laboratory is illustrated in Fig. 11. The ^{198}Au pulse height distribution (Fig. 12) was measured after TLD irradiation when the source activity had decreased to an acceptable level.

Special attention was paid to the encapsulation of the source material. Prior to irradiation, the chromium pellets used for TLD irradiation and for the pulse height distribution measurement were placed in separate polyethylene vials that were heat sealed to prevent accidental dispersal of radioactive material to the environment.

Table 2. Gamma-ray Sources Used in the Experimental Investigation

Nuclide	Half-life	Source Material	Primary Gamma-ray Energy, MeV
Cr-51	27.8 days	Chromium Pellets	0.32010
Au-198	2.7 days	Gold Foil	0.41180
Cs-137	30.0 yr	Cesium Metal	0.66164

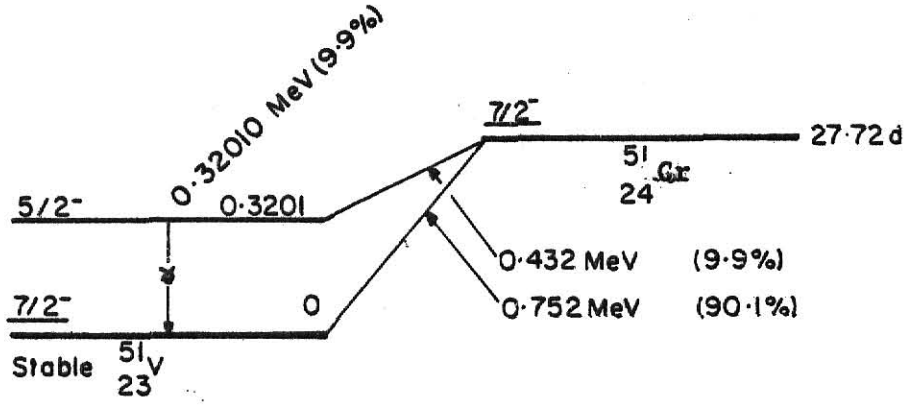

Fig. 8. Decay scheme for ^{51}Cr gamma ray source (from (32)).

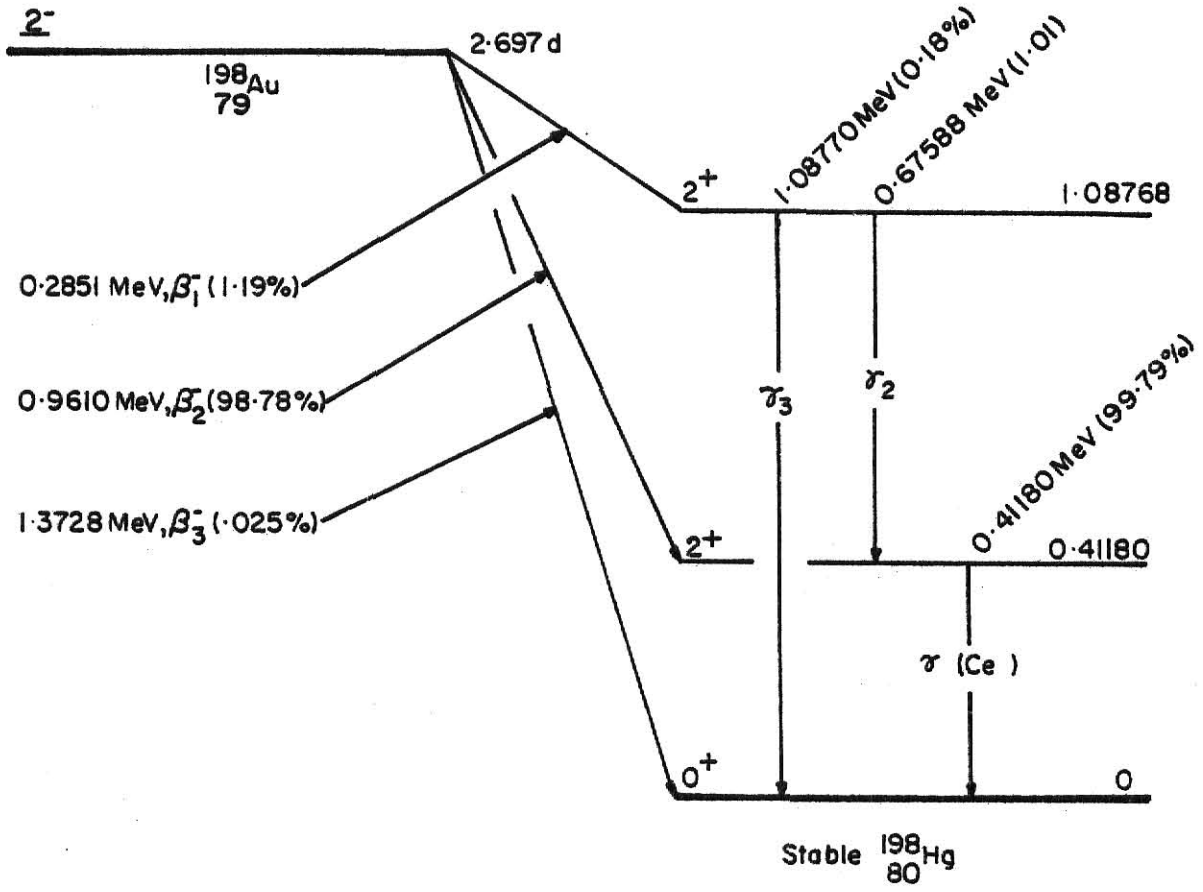

Fig. 9. Decay scheme for ^{198}Au gamma ray source (from (32)).

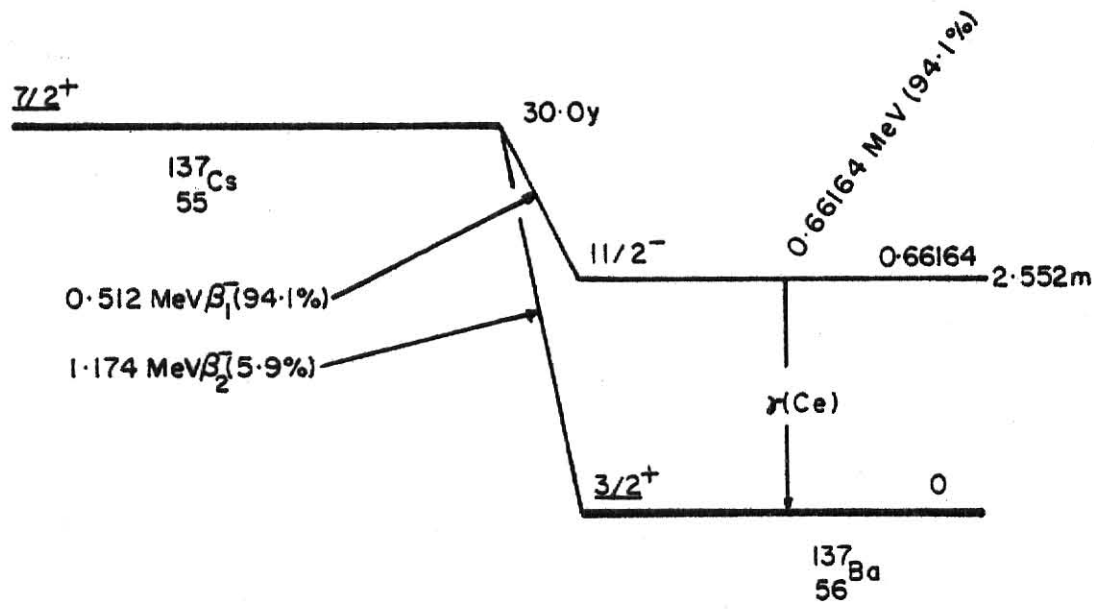

Fig. 10. Decay scheme for ^{137}Cs gamma ray source (from (32)).

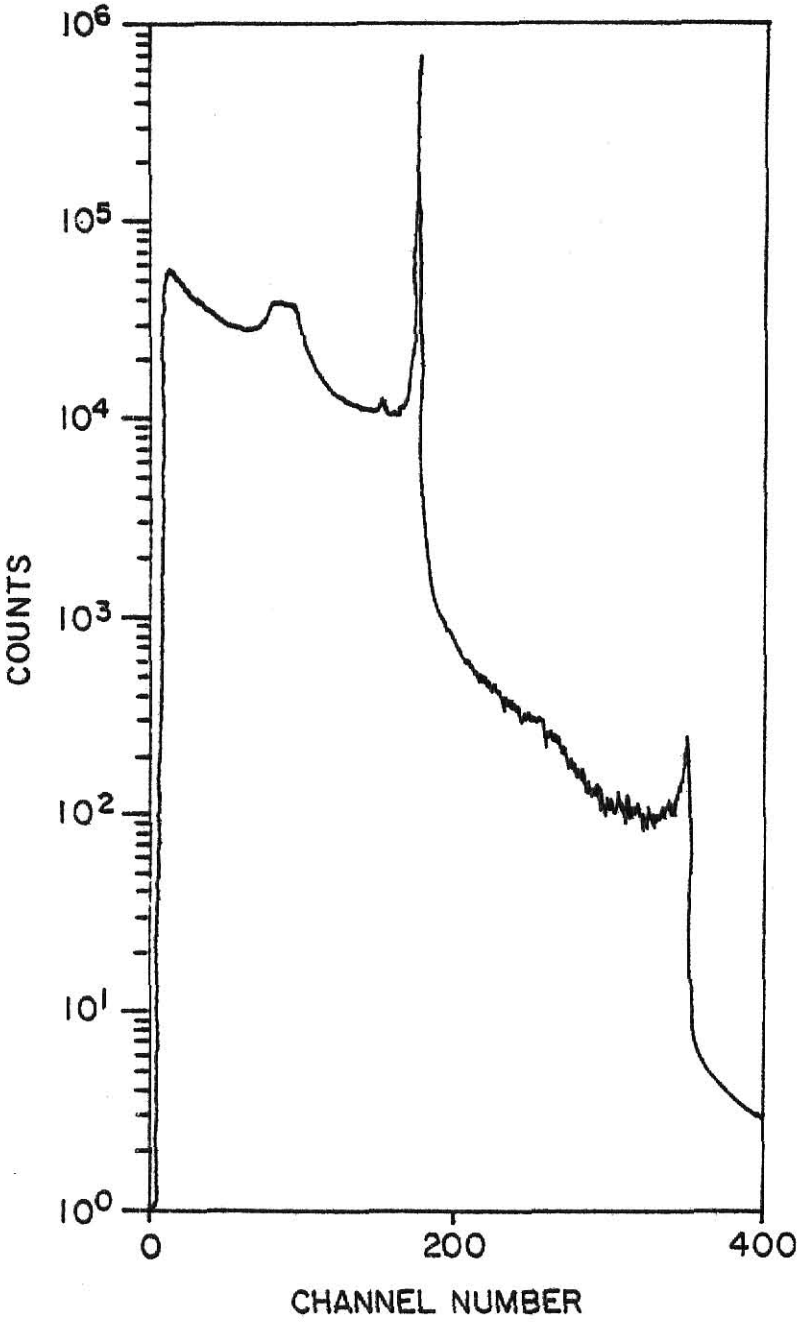

Fig. 11. Pulse height distribution of a 0.1 μCi ^{51}Cr source, (T_γ = 0.32010 MeV) (measured using the Ge(Li) system in the NAA Laboratory).

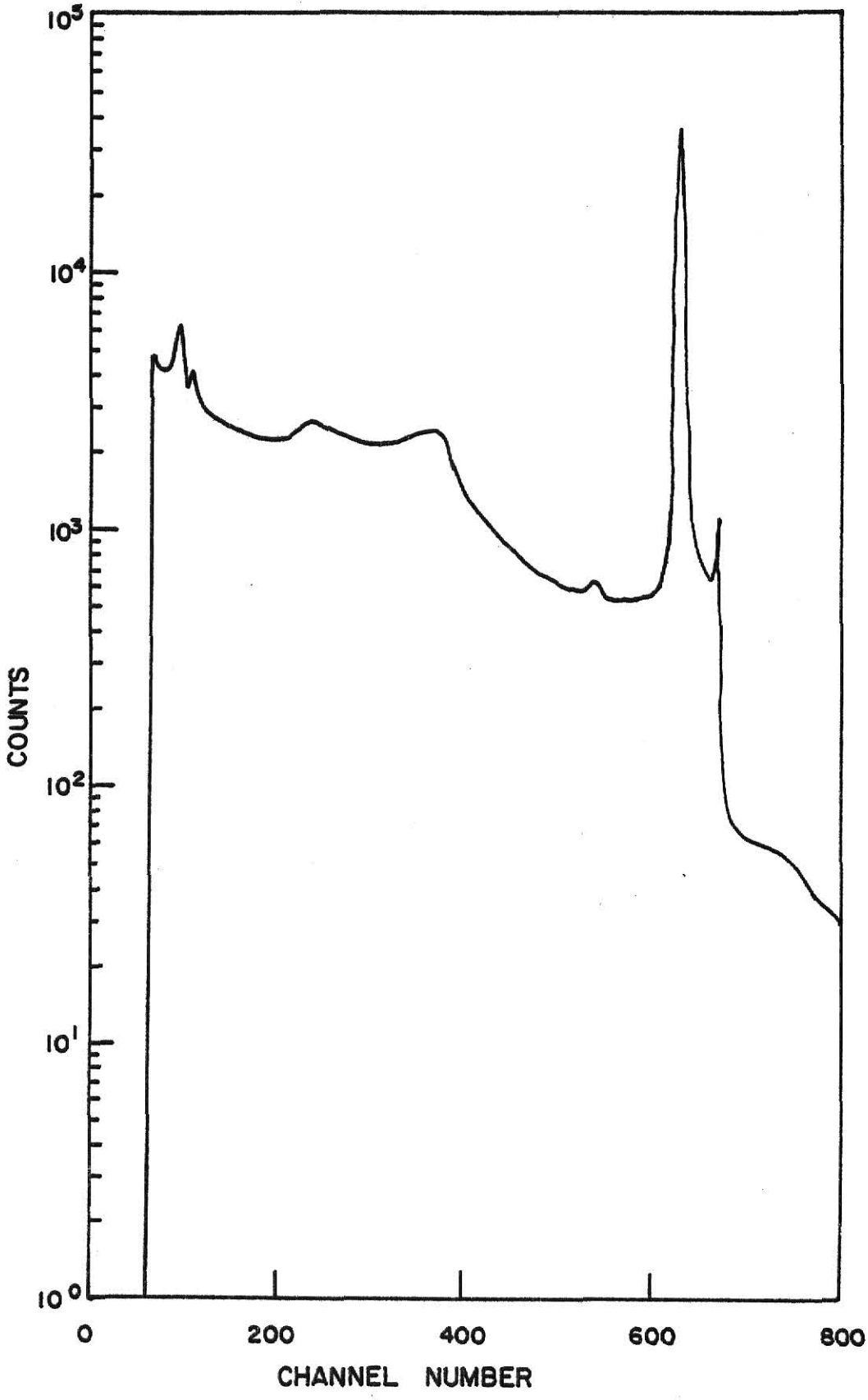

Fig. 12. Pulse height distribution of ^{198}Au source (T_γ = 0.41180 MeV) (measured using the Ge(Li) system in the NAA Laboratory).

Table 3. Location of source materials and irradiation times in the reactor for the production of nominal 3.0 mCi amounts of ^{51}Cr and ^{198}Au isotopes (reactor operation: 225 kW).

Isotope	Location of Source Material in Reactor	Quantity of Source Material (g)	Thermal Neutron Cross Section (b)	Irradiation Time (min)
^{51}Cr	Central thimble	4.8	16	240
^{198}Au	Rotary Specimen Rack (RSR)	0.10	98.8	11

The gold foil and the 3.0 mCi ^{137}Cs source were also encapsulated similarly. Prior to TLD irradiation for each source, each vial was placed in a larger vial and shut before placement on the irradiation device.

3.7 Determination of Dose Rate

Since all the encapsulated TLDs were subjected to the same total number of source decays for a particular gamma-ray source, an accurate determination of the source strength was not necessary. It was important, however, that bare and encapsulated TLDs received a large enough dose so that the TLD responses were well above the background current of the instrument. Table 4 lists typical responses that were obtained from ^{7}LiF and CaF_2:Mn TLDs irradiated by a nominal 3.0 mCi ^{137}Cs source, for an absorbed dose of approximately 0.5 rad in ^{7}LiF. The photomultiplier tube voltages used to obtain these responses were selected from considerations developed in Section 3.9. In both cases the responses obtained were well above background.

Given the approximate activity of each source used (3.0 mCi), an ideal location for the TLDs would be one in which the dose rate variation with distance was small. The dose rate at this location must also be sufficiently high so that the total irradiation time required to obtain 0.5 rad in ^{7}LiF (or CaF_2:Mn) was not excessive. A major portion of this study involved the irradiation of encapsulated TLDs, and irradiation to 0.5 rad in any one sleeve material would ensure at least 0.5 rad in ^{7}LiF or CaF_2:Mn (recall Figs. 4 and 5,

Table 4. Typical ^{7}LiF and CaF_2:Mn TLD responses for an absorbed dose of 0.5 rad in ^{7}LiF (3.0 mCi ^{137}Cs source).

TLD Type	Photomultiplier Tube Voltage (V)	First Readout (nC)	Second Readout (nC)	Background Readout Without TLD (nC)
^{7}LiF	600	2.201	0.135	0.093
CaF_2:Mn	500	30.8	0.460	0.134

Chapter 2, where the f ratios are consistently less than 1 for all sleeve materials in the energy range 0.1-0.7 MeV). Consequently, dose rates in iron were determined as a function of the radial distance from the source location. An analysis was made of the error in the dose rate due to an error in the TLD location. Since the source was located securely on the irradiation device, errors in source location were assumed negligible.

The dose rate, D(r), at a radial distance of r cm from a point source of strength S curies, in a material with an energy absorption coefficient $(\frac{\mu_{en}}{\rho})$ cm^2/g is given by

$$D(r) = \frac{CS}{4\pi r^2} \sum_{i=1}^{N} T_i \, y_i \, \frac{\mu_{en}}{\rho} \quad \text{(rad/hr)} \qquad (3.1)$$

where

T_i = Energy of i^{th} gamma of yield y_i per disintegration

C = Conversion factor = 1.602×10^{-8} rad -g/MeV.

According to this equation, the magnitude of the gradient of the dose rate, $|\frac{dD(r)}{dr}|$, decreases very rapidly with increasing r. Dose rates in iron due to a nominal 3.0 mCi ^{137}Cs source were computed as a function of r (see Fig. 13). It is seen that close to the source, where the gradient is changing very rapidly, a small positioning error would result in a large error in the dose rate. Far away from the source, where $|\frac{dD(r)}{dr}|$ is almost zero, a positioning error would have little effect on the dose rate. However, the dose rate would be too small. Based on a compromise between these two extremes, a

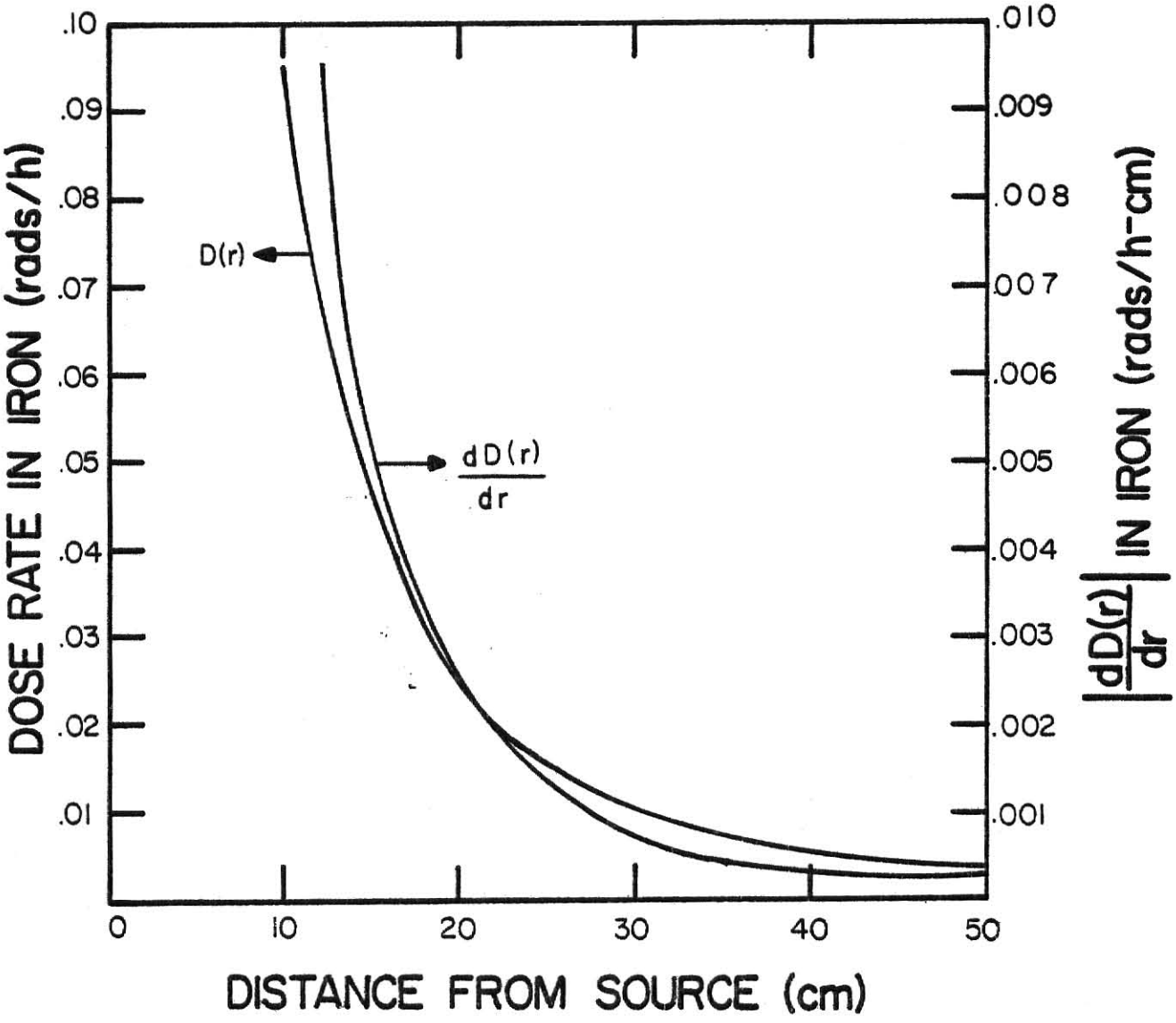

Fig. 13. Dose rates in iron (rads/hr), due to a nominal 3.0 mCi ^{137}Cs source, as a function of radial distance (cm) from the source location. Also included in the variation of the gradient of the dose rate $\left|\frac{dD(r)}{dr}\right|$ $(\frac{rads}{hr\text{-}cm})$ with source distance.

TLD location of 29 cm was chosen. A concentric groove was cut in the styrofoam sheet at this location.

Even though the groove was accurately cut in the styrofoam sheet, an error in the TLD location was possible. Figure 13 describes the variation of the gradient of the dose rate, $\left|\frac{dD(r)}{dr}\right|$, with the radial location, r. At the radial location of 29 cm, the magnitude of $\frac{dD(r)}{dr}$ is 0.0008 rad /hr-cm. The dose rate at this location is 0.0113 rad /hr. Assuming a maximum positioning error of 1 mm, the corresponding error in the dose rate at this location is less than 1%.

Bare and encapsulated TLD irradiation periods were scheduled for times exceeding 45 hours to achieve a desired absorbed dose of approximately 0.5 rad in the TLD and iron sleeve respectively. The actual irradiation times used for the ^{137}Cs, ^{198}Au, and ^{51}Cr gamma-ray sources are listed in Table 4 for both types of TLDs (bare and encapsulated).

3.8 Annealing Procedures

It has been found that the reproducibility of TLD responses is significantly affected by their annealing history. The annealing temperature and time must be consistent throughout their use, and investigators in the field had reported different procedures for various types of TLDs (22,23). The Harshaw Chemical Company recommended one hour at 400°C, followed by two hours at 100°C prior to irradiation of ^{7}LiF and CaF_2:Mn TLDs. Subsequent to irradiation,

Table 5. Irradiation times for bare and encapsulated TLDs irradiated by nominal 3.0 mCi ^{137}Cs, ^{198}Au, and ^{51}Cr gamma ray sources.

TLD Type	Irradiation Time (hrs)		
	^{137}Cs Source	^{198}Au Source	^{51}Cr Source
Bare ^{7}LiF (sort)	48	-	-
Encapsulated ^{7}LiF (all sleeves)	45	107	143
Bare CaF_2:Mn (sort)	48	-	-
Encapsulated CaF_2:Mn (all sleeves)	45	107	143

a ten minute anneal at 100°C was recommended in order to remove spurious peaks present in the glow curve at 80°C.[2] A wait period of twenty-four hours after irradiation also accomplishes the latter purpose.

Two ovens were used for the annealing procedure at Kansas State University. One was operated at 400°C and the other at 100°C. The 1x1x6 mm bare TLD rods were supported in an aluminum plate (150 x 120 x 15 mm) during annealing. Holes were drilled in the plate to support each individual TLD. The pre-irradiation annealing procedure was carried out in the following stages: one hour at 400°C; a ten minute wait period in an enclosed drawer; two hours at 100°C; followed by a wait period of one hour in the drawer. No appreciable temperature drop occurred when the TLDs and the aluminum plate were inserted in either oven. Simons (20) had obtained reproducible results using this annealing procedure.

3.9 Readout Equipment

Equipment supplied by the Harshaw Chemical Company was used for measuring the thermoluminescence (TL) from each TLD. As shown in Fig. 14, the equipment consisted of a Model 2000-A Thermoluminescence Detector coupled to a Model 2000-B Integrating Picoammeter. During readout, the bare TLD was supported on a heated planchet which was mounted inside a sliding drawer in the 2000-A unit. Light emitted by the TLD was converted into a current signal by the photomultiplier tube incorporated in the 2000-A unit. This current was then integrated

[2] M.Kaiseruddin (Major Professor : H.J.Donnert),M.S. Thesis, Kansas State University (1968).

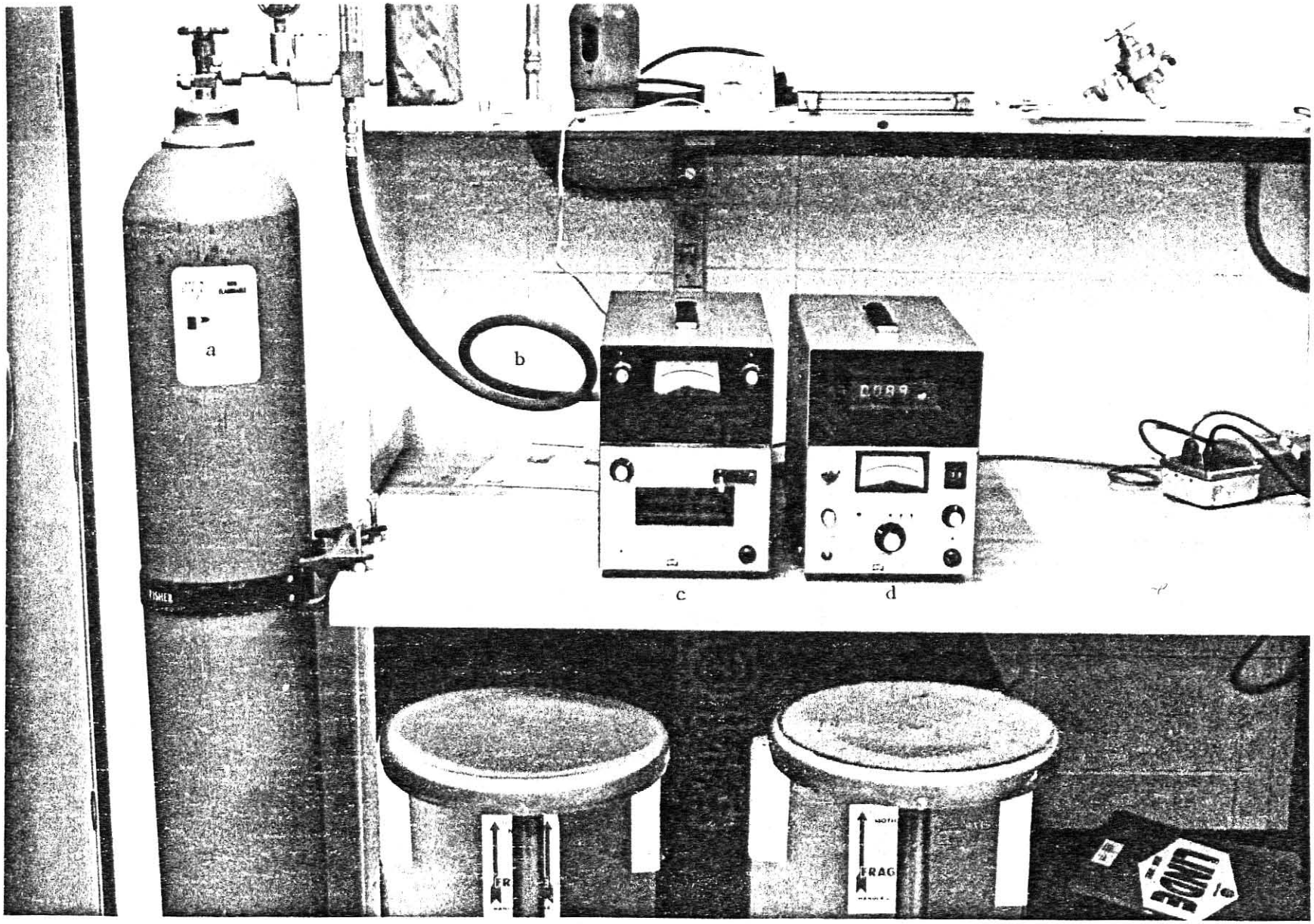

Fig. 14. Arrangement of readout equipment during readouts. (a) Carbon dioxide cylinder. (b) Carbon dioxide supply line to the 2000A unit. (c) Model 2000A Thermoluminescent Analyzer. (d) Model 2000B Integrating Picoammeter.

and the charge displayed by the 2000-B unit. Additional analog outputs were also available from both units. A dc voltage output signal was available from the 2000-A unit which was proportional to the temperature of the heated planchet. Linear and logarithmic dc voltage signal outputs were provided by the 2000-B unit for recording the time-dependent current output of the photomultiplier tube (i.e., the glow curve). Inert gas (such as nitrogen or carbon dioxide) was circulated over the planchet to reduce nonradiation induced thermoluminescence.

A sectional view of the 2000-A unit is shown in Fig. 15. The built-in light source, which consisted of ^{14}C activated NaI(Tl), moved into position when the sample drawer was fully extended. It was used for routine checks on photomultiplier tube gain and system stability. The optical filters, lenses and mirror served to modify the light path and prevent infra-red radiation from the sample heater from entering the photomultiplier tube. The photomultiplier tube was housed in a cooling jacket and provided with electrostatic and magnetic shielding. In order to keep the background current from the photomultiplier tube low and uniform, a thermoelectric cooler maintained the tube at a constant 50°F.

Linear heating of the planchet was achieved by means of the PRE and TEMP potentiometers located at the rear of the 2000-A unit. The PRE control established the maximum preheat temperature, and the TEMP control was used to set the subsequent linear heating rate. The maximum heater temperature was selected by the HEATER TEMPERATURE

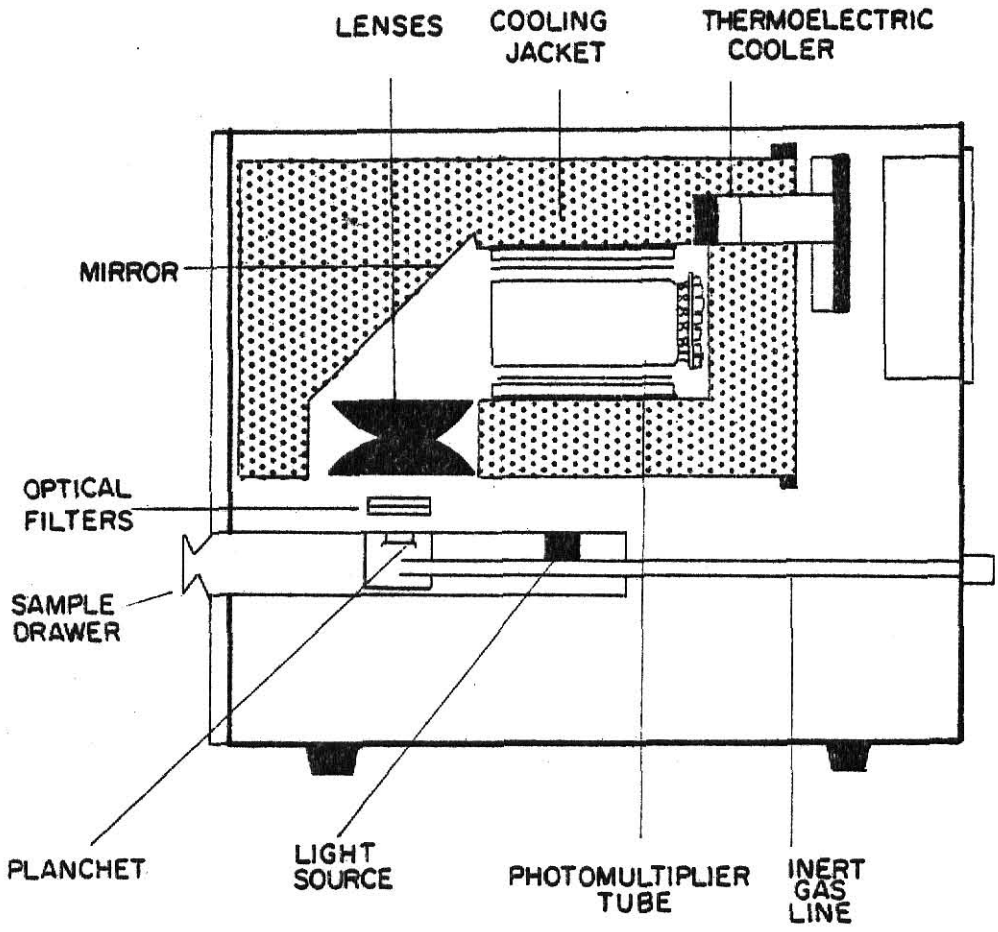

Fig. 15. Model 2000A Thermoluminescent Analyzer.

MAX control located on the front panel. The Harshaw Chemical Company recommended a 100°C preheat for ^{7}LiF TLDs, followed by a linear heating rate of 10°C/sec to a maximum temperature of 240°C, as shown in Fig. 16. For CaF_2:Mn TLDs, the maximum heater temperature was 350°C, and the temperature profile was similar. A 30 sec heating period was used for both type TLDs.

The current signal from the photomultiplier tube was integrated and displayed as a total charge on the 2000-B unit. The current meter on the front panel was calibrated to read over an eight-decade range (from 10^{-13} to 10^{-6} amperes). The PERIOD switch located on the front panel regulated the charge integration period and the planchet heating period. The HIGH VOLTAGE potentiometer on the front panel established the photomultiplier tube voltage. This control was provided with a locking device to prevent any accidental changes in the voltage during operation.

The operating voltages of the photomultiplier tube, used for measuring ^{7}LiF and CaF_2:Mn TLD readouts, were determined from signal-noise curves supplied by the Harshaw Chemical Company. These signal-noise curves described the variation of the signal and noise currents with photomultiplier tube voltage (Fig. 17). The signal-to-noise ratio (SNR) increased gradually with voltage up to 700 volts, after which the increase was less gradual. Thus, it was seen that operating the tube at voltages higher than 700 volts would be of little benefit. On the contrary, photomultiplier tube fatigue would be a factor at

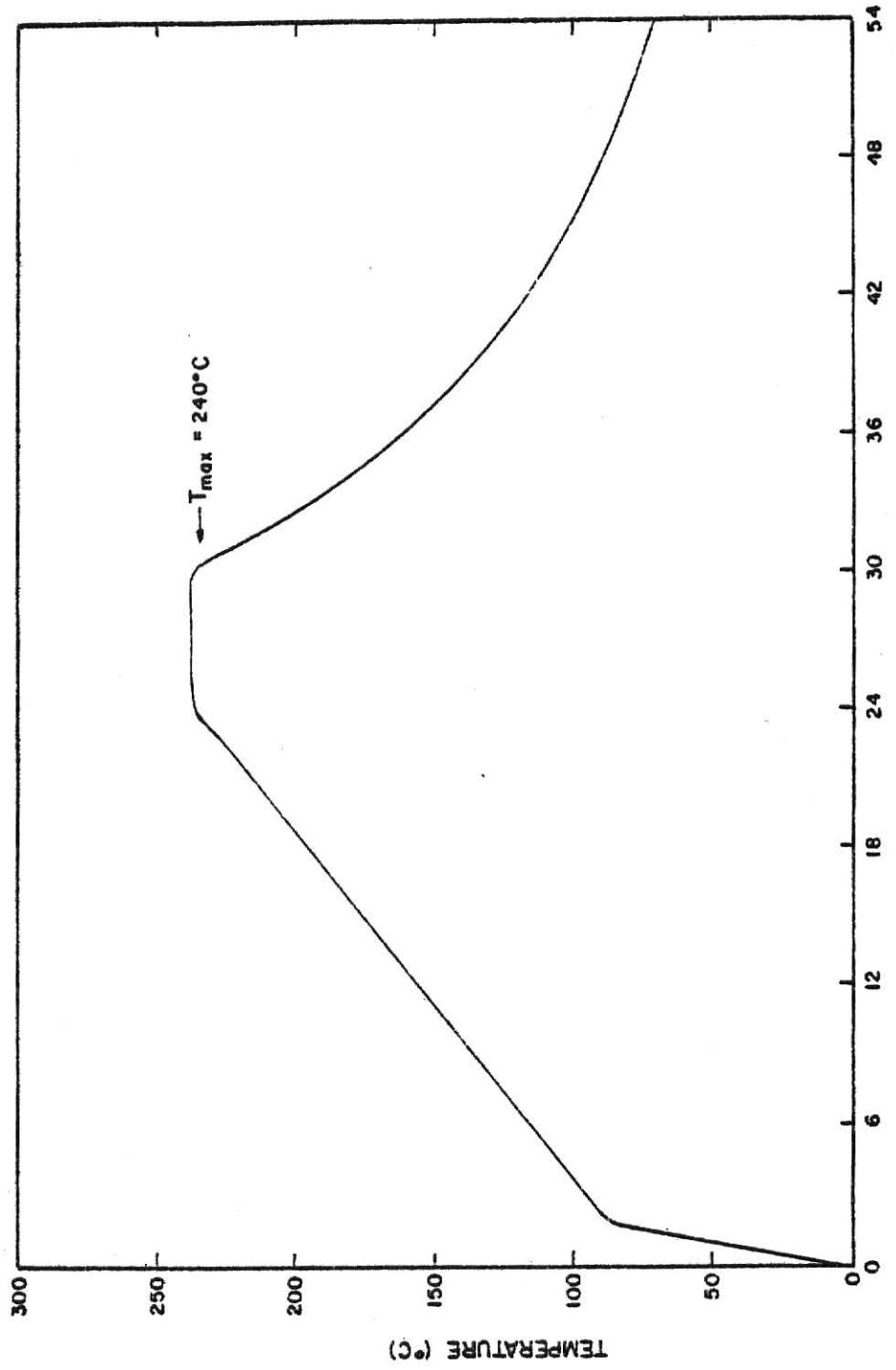

Fig. 16. Temperature profile established for the heating planchet in the 2000-A unit for use with the readout of ^{7}LiF TLDs.

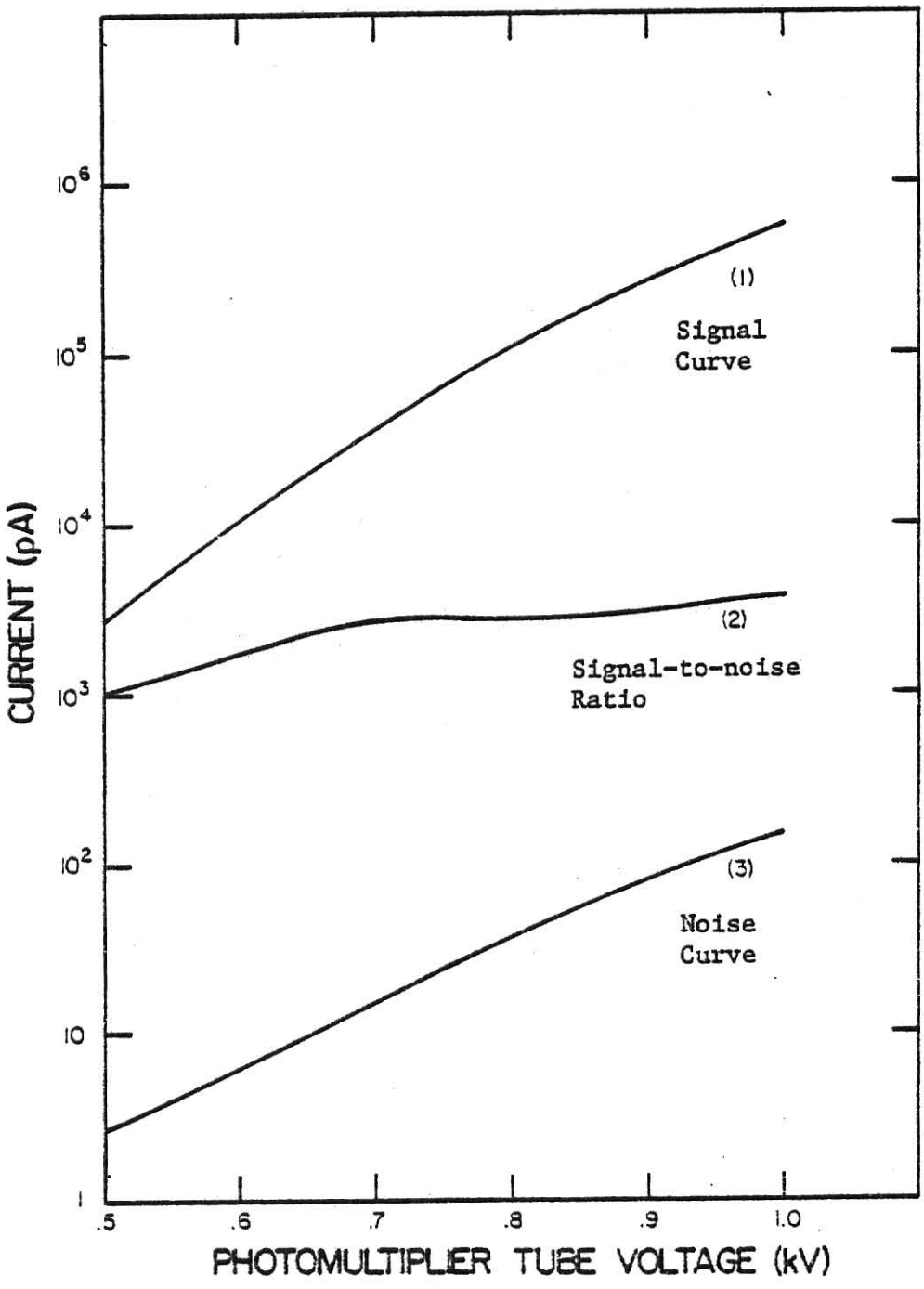

Fig. 17. Signal-noise curves for the photomultiplier tube (Type 9856T) in the Model 2000-A unit (data supplied by the Harshaw Chemical Company).

these high voltages. A voltage of 600 V was chosen for use with ^{7}LiF TLDs to obtain currents of adequate levels and to minimize photomultiplier tube fatigue. Since CaF_2:Mn TLDs emit more TL per unit dose than ^{7}LiF (see Table 4), a lower voltage setting of 500 V was chosen to futher minimize photomultiplier tube fatigue.

Systematic procedures were established for the setup of the equipment prior to measuring light emission from TLDs. These are discussed in the following section.

3.10 Initial Setup

Prior to obtaining data from TLDs, a systematic checkout procedure was established for the instrumentation. This procedure was followed throughout the experimental program in order to obtain consistent results, and minimize experimental error due to improper use of equipment. The following sequence of operations was performed prior to measuring readouts:

(i) Turn the analyzer on, insert the planchet drawer, and wait for a minimum of one day to obtain temperature equilibrium.

(ii) Set the photomultiplier tube voltage, by turning the meter control knob on the 2000-B unit to HV and adjust the HV control to 600 V (for ^{7}LiF TLDs) or 500 V (for CaF_2:Mn TLDs).

(iii) Set the period switch to 30 sec on the 2000-B unit.

(iv) Set the range, ampere control to auto on the 2000-B unit.

(v) Adjust the carbon dioxide flow to 10 cu ft/hr.

(vi) Zero the electrometer on the 2000-B unit by flipping the multiplier switch to the 0.1 position and back again to the x 1 position. Adjust the zero control until the needle on the electrometer stays stationary when the multiplier switch is flipped back and forth between the two positions. Return the multiplier switch to the x 1 position after zeroing the electrometer.

(vii) Set the meter switch to the current mode and adjust the current suppression knob on the rear panel of the 2000-B unit for a current of 3 picoamperes.

(viii) Slide the 1 mA-100 mV switch on the rear panel of the 2000-B unit to the 100 mV position. Attach the temperature output cable (from the rear of the 2000-A unit) to the X-Y recorder. Set the horizontal time sweep on the recorder to 5 sec/in and the vertical axis to 10 mV/in. When analyzing ^{7}LiF TLDs, adjust the temperature rate, pre-heat (rear panel of 2000-A unit) and heater maximum (front panel of 2000-A unit) controls until the temperature profile matches the profile shown in Fig. 16. Use a similar profile for CaF_2:Mn TLDs except for the maximum temperature of 350°C.

(ix) With the planchet drawer inserted, measure and record the dark-current charge five times using a 30 second period. Wait for the planchet temperature to drop to 50°C (approximately 1 minute for ^{7}LiF, and 1.5 minutes for the CaF_2:Mn temperature profiles) prior to each measurement. The average dark current should be less than 0.5 nC/sec in each case.

(x) Pull the planchet drawer out, measure and record the output from the built-in light source over a 10 second period. These readings should average nominally 314 nC at 600 V and 57 nC at 500 V.

(xi) Attach the linear output cable on the 2000-B unit to the X-Y recorder. Set the horizontal time sweep to 5 sec/in and the vertial axis to 20 mV/in.

The system is now ready for recording glow curves on the X-Y recorder and displaying the total light output as an LED readout on the 2000-B unit simultaneously.

In the event that the system is turned off for any reason, the initial setup procedure (steps (i) through (xi) above) must be repeated prior to analyzing the TLDs.

3.11 Analyzer Operation

After initial setup was completed, the system was ready for measuring TLD readouts. It was necessary to establish and maintain a systematic and reproducible sequence of operations to minimize systematic errors. The established sequence of operations is described below:

(i) Zero the electrometer prior to analyzing the TLDs and every hour thereafter.

(ii) Check the carbon dioxide flow rate for a flow of 10 cu ft/hr.

(iii) Turn the X-Y recorder on, if measurement of the glow curve is desired. If not, the X-Y recorder may be turned off.

(iv) Read out the TLD over a 30 second period. Wait until the planchet temperature drops to 50°C (1 minute for ^{7}LiF, and 1.5 minutes for CaF_2:Mn TLDs) and read out the TLD again. Wait until the temperature drops below 100°C before removing the TLD and inserting a new one. The readout cycles used for ^{7}LiF and CaF_2:Mn TLDs are illustrated in Table 6.

3.12 Sensitivity Selection

Bare TLDs, subjected to the same average absorbed dose, do not produce an identical response, even if they are fabricated from the same batch of material. Significant improvements in precision were reported in the literature (19,20) when these differences, which were largely statistical in nature, had been corrected for in experimental investigations. The correction procedure is referred to as sensitivity selection. Briefly, sensitivity selection involves the irradiation of TLDs from a single batch of material to the same average absorbed dose, and discarding those TLDs that differ by more than a given percentage in their response from the group mean response. The purpose of the sensitivity selection procedure was to select a subset of TLDs with individual sensitivites that be as close as was practically possible to the final subset mean.

The sensitivity selection procedure had been incorporated in a computer code, SAD, developed at the Argonne National Laboratory by Dr. G. G. Simons. A flow chart depicting the logic incorporated in the sensitivity selection section of the program is shown in

Table 6. Readout cycles used for the analysis of ^{7}LiF and CaF_2:Mn TLDs.

Elapsed Time (min)		
^{7}LiF TLDs	CaF_2:Mn TLDs	Operation Description
0	0	Load TLD, close drawer, initiate first readout
0.5	0.5	End of read cycle
1.5	2.0	Temperature below 50°C. Initiate second readout
2.0	2.5	End of second read cycle
2.5	3.25	Remove TLD, insert new TLD, close drawer
3.0	4.0	Initiate readout of new TLD

Appendix A. Initially, the TLD responses were arranged in the order of decreasing sensitivity. The mean and standard deviation of the ordered set was then computed, together with a 5% band about the mean of the set. The 5% selection criterion had been used largely from the viewpoint of selecting as many TLDs as possible with relatively good precision, and not from any rigorous statistical considerations. The largest and smallest responses were compared to the mean response, and if the deviations in both cases were within the band, the selection process was bypassed and the entire batch was accepted as the precision set. If, however, the deviations in either or both cases were outside the band, the TLD response with the greater deviation from the mean was discarded. The mean, standard deviation, and selection limits for the reduced set were recomputed, and comparisons were made with the largest and smallest responses, as before. The final precision set of TLDs, obtained after successive discards, was then used for future investigations with correction factors computed for all TLDs. The correction factor for each TLD was the ratio of the response to the mean of the final precision set.

The same procedure was used at Kansas State University for selecting a precision subset for both ^{7}LiF and CaF_2:Mn TLDs. A batch of approximately 220 TLDs was pre-annealed using the procedure discussed in Section 3.8. After annealing, the TLDs were placed in the circular groove in the irradiation device, and successive TLDs were located at least 3mm apart. A 3.0 mCi ^{137}Cs

source was placed in the center of the circle, and the irradiation device was raised to a height of ten feet from the floor. For CaF_2:Mn TLDs, black paper was used to protect the TLDs from ambient light during irradiation. After irradiation to nominally 0.5 rads, the TLDs were removed and placed in numbered, opaque, brown envelopes and stored for 24 hours in an enclosed cabinet prior to readout. During readout, individual TLDs were removed from their envelopes one at a time and placed on several layers of soft tissue, as part of the readout cycle. For CaF_2:Mn TLDs, only incandescent lighting was used during readout, and individual TLDs were covered with black paper prior to readout to serve as protection against the incandescent lighting.

The TLD identification together with its readout was used as input for the SAD code to obtain a precision set. The spread of the TLD readouts about the final precision subset mean is illustrated in Figs. 18 and 19, respectively, for the ^7LiF and CaF_2:Mn TLDs. The TLDs whose responses lay within the 5% band about the final subset mean were accepted as the final precision set. The rest of the TLDs were discarded. Nominally 59% and 66%, respectively, of the original batch of ^7LiF and CaF_2:Mn TLDs were accepted as the precision set.

3.13 Procedures for Encapsulated TLDs

The precision subsets obtained for both types of TLDs, as discussed in Section 3.12, were used for all subsequent irradiations. Each subset was partitioned into groups of nominally 15 TLDs and a

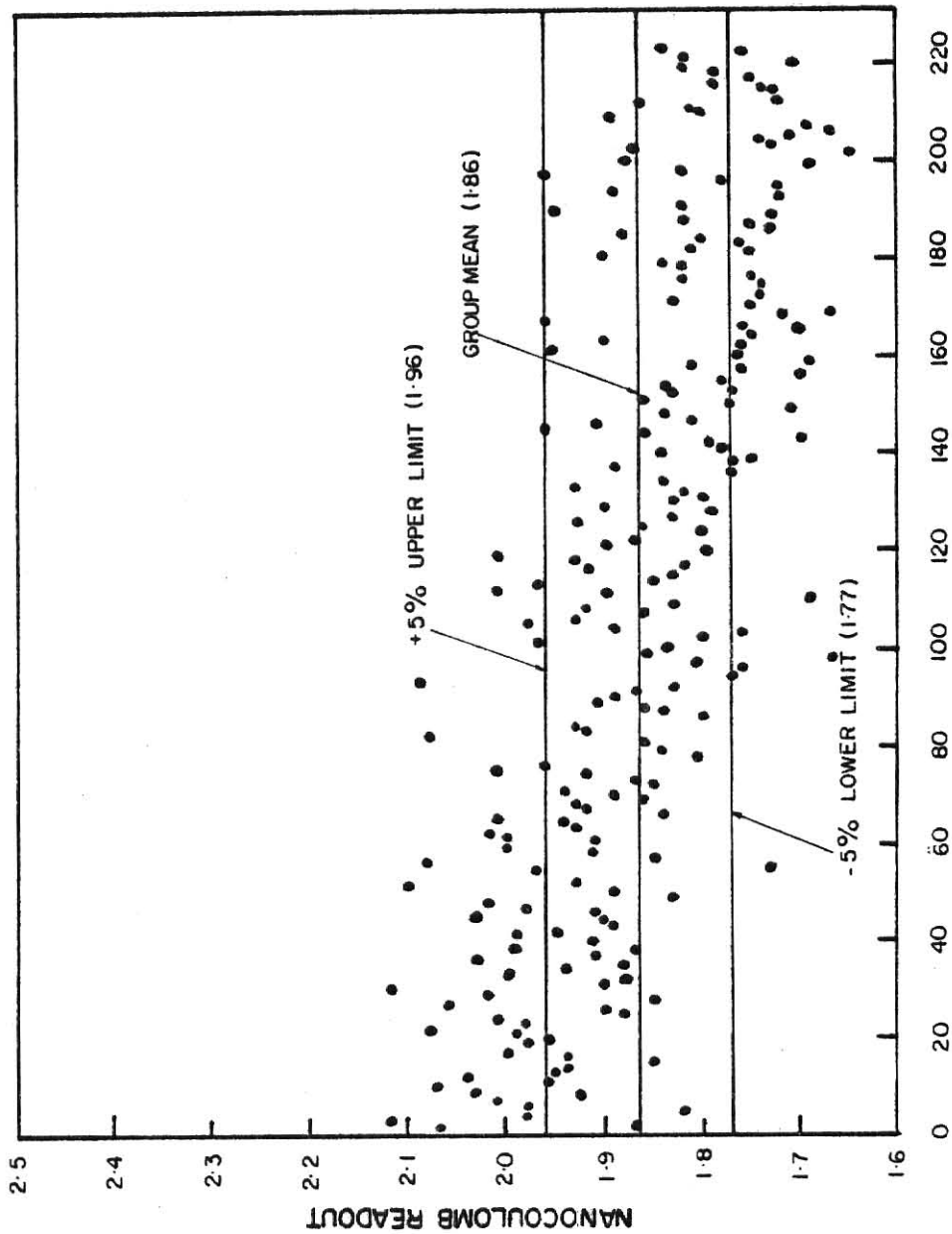

Fig. 18. Distribution of ^{7}LiF TLD readouts about the final precision subset mean (sensitivity selection procedure).

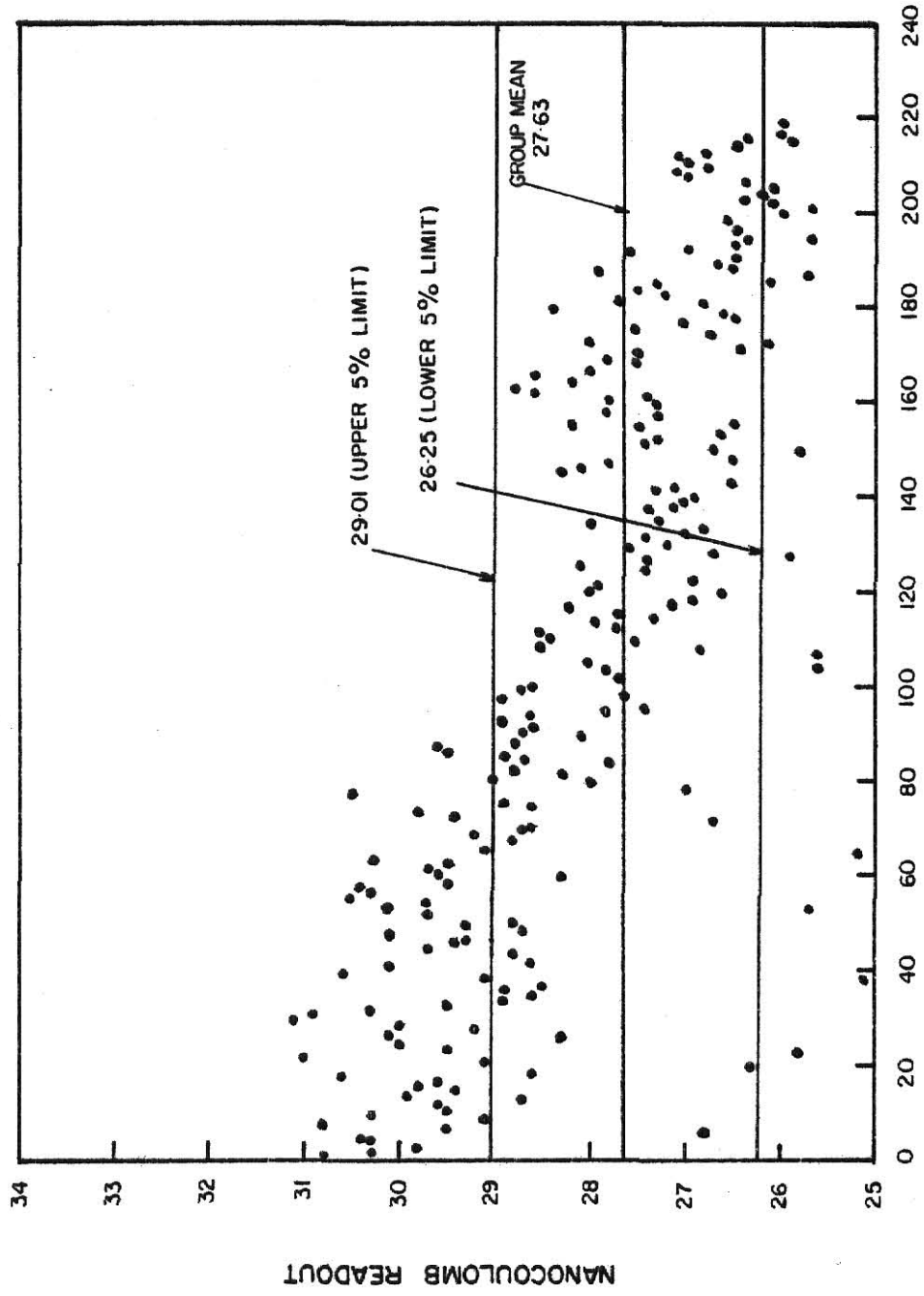

Fig. 19. Distribution of CaF_2:Mn TLD readouts about the final precision subset mean (sensitivity selection procedure).

particular type of sleeve material was assigned to each group. This ensured that all TLDs encapsulated by the same type of sleeve material had similar sensitivity correction factors. Table 7 lists the sleeves used in the investigation at Kansas State University. Each sleeve was a 12.7 mm long hollow cylinder, and the hole diameter at either end was sufficient to hold the 1x1x6 mm TLD. Plugs made of the same material were inserted at both ends.

During irradiation, encapsulated TLDs were placed on the circular groove cut in the styrofoam sheet. TLDs that were encapsulated by the same type sleeve were located together. The spacing between each sleeve was at least 5 mm. The gamma-ray source was located at the center of the circle. Irradiation times were adjusted to obtain a total absorbed dose of approximately 0.5 rad in iron, as listed in Table 5, Section 3.7. Following irradiation, encapsulated TLDs were placed in individual, opaque envelopes and stored in an enclosed cabinet for 24 hours.

Subsequent to initial setup of the equipment (see Section 3.10), TLDs were read out sequentially, without interruption, using the procedure outlined in Section 3.11. Just prior to being placed inside the TLD analyzer, individual TLDs were removed from their sleeves as part of the readout cycle.

After all the data had been gathered, the mean and standard deviation of the TLD responses (corrected for background) were computed for each type sleeve material, and for both sorted and un-

Table 7. Encasement Materials Used During Measurement of the Energy Response of Encased ^{7}LiF and CaF_2:TLDs.

Material	Quantity	Atomic Number	Density (g/cm^3)	Hole Diameter (cm)	Wall Thickness (g/cm^2)
Lead	9	82	11.34	.22	0.734
Tantalum	10	73	16.60	.22	0.696
Tin	15	50	7.30	.22	0.608
Copper	14	29	8.96	.25	0.694
Iron	16	26	7.87	.22	0.656
Stainless Steel	17	Std ANL	7.80	.22	0.693
Aluminum	8	13	2.70	.22	0.514

sorted TLDS. The mean and standard deviation were obtained from:

$$\bar{X}_M = \sum_{i=1}^{N} \frac{X_i}{N} \tag{3.2}$$

$$\sigma_M^2 = \sum_{i=1}^{N} \frac{(X_i - \bar{X}_M)^2}{N-1} \tag{3.3}$$

where

$\bar{X}_M$ = mean response of N TLDs encapsulated by sleeve material of type M.

σ_M = standard deviation of the mean of the N TLD readouts.

X_i = response of the i-th TLD (i=1, ... N).

The mean and standard error of the mean ($\sigma_M/\sqrt{N}$) are reported for each type sleeve, gamma-ray source and TLD in Section 4.4. An uniform notation was used to report the results. Since the TLD response is directly proportional to the absorbed dose in the TLD, the $\bar{X}_M$ values were reported as ${}_mE^{exp}_{D(M)}$, where

${}_mE^{exp}_{(D(M)}$ = experimentally obtained absorbed dose per unit mass (m) in the TLD encapsulated by a sleeve of type M.

This type of notation was used to ensure consistency in terminology when comparisons are made between theory and experiment. These comparisons are discussed in the next chapter.

4.0 RESULTS AND DISCUSSION

4.1 General Considerations

Data collected in this investigation were in the form of responses measured, using two types of encapsulated TLDs, as a function of sleeve material and gamma-ray energy. Nominally 500 TLD responses were obtained using both types of TLDs. This does not include the additional 450 TLD responses obtained during the sensitivity selection procedure. To synthesize this information and present the results in a convenient, readily accessible form, the mean TLD responses, together with their standard errors, are reported for each sleeve irradiated by a gamma-ray source. Theoretical results are also synthesized and reported for the same gamma energies. The degree of agreement between experiment and theory is also included in this chapter, as well as an intercomparison between results reported at Argonne National Laboratory (ANL) and those obtained in this study.

For convenience of presentation, the material in this chapter is presented in several sections. Section 4.2 describes the method used to compare the experimental results and theoretical predictions of absorbed dose in the encapsulated TLDs. The theoretical results obtained from the TERC/III code are presented in Section 4.3. Experimental results obtained in this investigation are presented in Section 4.4. Experimental and theoretical comparisons are made in Section 4.5 for each TLD material. Intercomparisons with the ANL results are described in Section 4.6.

4.2 Development of Experimental and Theoretical Comparisons

A relative method of comparison was used to compare the theoretically predicted and experimentally observed doses in the encapsulated TLDs. As was mentioned in Section 3.7, all encapsulated TLDs were exposed to the same total number of source decays for a particular gamma-ray source. It was therefore possible to normalize the mean TLD response for each sleeve material to the mean TLD response for a reference sleeve, and compare these normalized results with the corresponding normalized theoretical results. The use of this relative method of comparison eliminated the necessity of accurately determining the strengths of the individual gamma-ray sources. This procedure removed a source of systematic error that may have influenced the results.

Under uniform irradiation by a monoenergetic gamma-ray source of energy T_γ MeV, the calculated absorbed dose in the encapsulated TLD is related to the calculated sleeve dose by

$$ {}_{m}E_{D(M)}^{calc} = f(T_\gamma)\ {}_{m}E_{M}^{calc} \qquad (4.1) $$

where

${}_{m}E_{D(M)}^{calc}$ = calculated absorbed dose per unit mass (m) in the TLD encapsulated by a sleeve of material M.

$f_M(T_\gamma)$ = f ratio for sleeve of material M (from TERC/III code, discussed in Section 2.2.6).

${}_{m}E_{M}^{calc}$ = calculated absorbed dose per unit mass (m) in the sleeve of material M.

For a total irradiation time of t secs, the absorbed dose in the sleeve (rads) is given by,

$$ {}_{m}E_{M}^{calc} = \frac{KS}{4\pi r^2} T_\gamma \left(\frac{\mu_{en}(T_\gamma)}{\rho}\right)_M \exp\left(-\left(\frac{\mu_{en}(T_\gamma)}{\rho}\right)_M t_M\right) \qquad (4.2) $$

where

K = Conversion factor = 1.602×10^{-8} (rad-g/MeV)

S = total number of source decays = activity $(\frac{1}{sec})$ x t (secs).

r = radial location of encapsulated TLD (cm).

$\left(\frac{\mu_{en}(T_\gamma)}{\rho}\right)_M$ = mass energy absorption coefficient for a sleeve of material M (cm^2/g).

t_M = sleeve thickness (g/cm^2).

Since S and r were held constant for all sleeves during irradiation with each gamma-ray source, Eq. 4.2 simplifies to,

$$ {}_{m}E_{M}^{calc} = C \left(\frac{\mu_{en}(T_\gamma)}{\rho}\right)_M \exp\left(-\left(\frac{\mu_{en}(T_\gamma)}{\rho}\right)_M t_M\right) \qquad (4.3) $$

where C is a constant. Combining Eqs. (4.1) and (4.3) yields,

$$ {}_{m}E_{D(M)}^{calc} = C\, f_M(T_\gamma) \left(\frac{\mu_{en}(T_\gamma)}{\rho}\right)_M \exp\left(-\left(\frac{\mu_{en}(T_\gamma)}{\rho}\right)_M t_M\right) . \qquad (4.4) $$

Neglecting the exponential attenuation of the primary gamma-rays in the sleeve material, Eq. (4.4) reduces to,

$$ {}_{m}E_{D(M)}^{calc} = C\, f_M(T_\gamma) \left(\frac{\mu_{en}(T_\gamma)}{\rho}\right)_M . \qquad (4.5) $$

Normalized to a reference sleeve material of type R, Eqs. (4.4) and (4.5) become,

$$ {}_{m}E^{calc}_{D(M)}\ (\text{norm.}) = \frac{f_M(T_\gamma)\ (\frac{\mu_{en}(T_\gamma)}{\rho})_M\ \exp(-(\frac{\mu_{en}(T_\gamma)}{\rho})_M\ t_M)}{f_R(T_\gamma)\ (\frac{\mu_{en}(T_\gamma)}{\rho})_R\ \exp(-(\frac{\mu_{en}(T_\gamma)}{\rho})_R\ t_R)} \qquad (4.6) $$

$$ {}_{m}E^{calc}_{D(M)}\ (\text{norm.}) = \frac{f_M(T_\gamma)\ (\frac{\mu_{en}(T_\gamma)}{\rho})_M}{f_R(T_\gamma)\ (\frac{\mu_{en}(T_\gamma)}{\rho})_R} \qquad (4.7) $$

Equations (4.6) and (4.7) served as the basis for computing the normalized theoretical results for each sleeve material as a function of gamma-ray energy, for both TLD materials.

The mean encapsulated TLD response for each sleeve, together with its standard error (described in Section 3.13), was also normalized to the reference sleeve material R to obtain,

$$ {}_{m}E^{exp}_{D(M)}\ (\text{norm}) = \frac{{}_{m}E^{exp}_{D(M)}}{{}_{m}E^{exp}_{D(R)}} \pm \sigma_R \qquad (4.8) $$

where

${}_{m}E^{exp}_{D(M)}\ (\text{norm})$ = ${}_{m}E^{exp}_{D(M)}$ normalized to the mean encapsulated TLD response for the reference sleeve of material R.

σ_R = error of the ratio.

The error of the ratio, σ_R, is determined from (see Reference (34)),

$$ \sigma_R = {}_{m}E^{exp}_{D(M)}\ (\text{norm}) \left[(\frac{\sigma_M}{{}_{m}E^{exp}_{D(M)}})^2 + (\frac{\sigma_R}{{}_{m}E^{exp}_{D(R)}})^2 \right]^{\frac{1}{2}} \qquad (4.9) $$

The ratio of Eq. (4.6) to Eq. (4.8) (with attenuation correction applied) served as a measure of agreement between calculations and

experiment, described by,

$$\left(\frac{C}{E}\right) = \frac{{}_{m}E^{calc}_{D(M)}\ (norm)}{{}_{m}E^{exp}_{D(M)}\ (norm)}$$

$$= \frac{f_M(T_\gamma)\ \left(\frac{\mu_{en}(T_\gamma)}{\rho}\right)_M \exp\left(-\left(\frac{\mu_{en}(T_\gamma)}{\rho}\right)_M t_M\right)\ {}_{m}E^{exp}_{D(R)}}{f_R(T_\gamma)\ \left(\frac{\mu_{en}(T_\gamma)}{\rho}\right)_R \exp\left(-\left(\frac{\mu_{en}(T_\gamma)}{\rho}\right)_R t_R\right)\ {}_{m}E^{exp}_{D(M)}} \qquad (4.10)$$

Neglecting the exponential attenuation of the primary gamma-rays in all sleeve materials, Eq. (4.10) reduces to,

$$\left(\frac{C}{E}\right) = \frac{f_M(T_\gamma)\ \left(\frac{\mu_{en}(T_\gamma)}{\rho}\right)_M\ {}_{m}E^{exp}_{D(R)}}{f_R(T_\gamma)\ \left(\frac{\mu_{en}(T_\gamma)}{\rho}\right)_M\ {}_{m}E^{exp}_{D(M)}} \ . \qquad (4.11)$$

C/E ratios close to unity represented good agreement between experiment and theory.

4.3 Theoretical Results for ^{7}LiF and CaF_2:Mn TLDs

Absorbed doses in both types of TLD materials were calculated, for all types of sleeve materials being investigated, as a function of gamma-ray energy using the TERC/III computer code. The TERC/III results used in this study were in the form of the expression represented by Eq. (4.5) where the constant C was set to unity. Computation of $f(T_\gamma)$ was carried out in the code through the use of Eq. (2.19). Collision mass stopping power ratios (CMSP's) for the dosimeter and sleeve, used in Eq. (2.19), were calculated using the equation given

by Berger and Seltzer (35). The input parameters to the code for the TLD materials and each sleeve are illustrated in Tables 8 and 9. The density effect parameters listed were used in the calculation of the CMSP's. The CMSP's calculated by TERC/III were within 1% of the values reported by Berger and Seltzer for ^{7}LiF and CaF_2:Mn TLDs, over the energy range under investigation (36).

A consistent set of mass energy absorption coefficients, $\frac{\mu_{en}(T_\gamma)}{\rho}$, were selected for each sleeve material by using the values published in the Nuclear Data Tables (37). These coefficients were derived from the total absorption coefficients, $\sigma_a(tot)$, listed in Ref. (37) as follows,

$$\sigma_a(tot) = \sigma_a(incoh) + \sigma_a(photo) \ (\frac{barns}{atom}) \ . \qquad (4.12)$$

where

$\sigma_a(incoh)$ = incoherent (absorption) Compton cross section.

$\sigma_a(photo)$ = photoelectric absorption cross section.

Appropriate conversion factors were used to convert $\sigma_a(tot)$ from (barns/atom) to (cm^2/g) for each sleeve material. Uncertainties reported for $\sigma_a(incoh)$ and $\sigma_a(photo)$ were nominally 10% (exact figures were not given), leading to a corresponding uncertainty in $\sigma_a(tot)$ of nominally 15%. Since the errors involved in the calculation of $f(T_\gamma)$ and in $\sigma_a(tot)$ were difficult to estimate, errors were not assigned to the calculated absorbed doses obtained from the TERC/III code.

TERC/III results are illustrated in Tables 10-15 for both TLD materials (column (2)), where the sleeve materials are arranged in the order of decreasing atomic number. A significant trend is observed in these results, namely, that the calculated TLD absorbed dose increases with increasing sleeve atomic number. The reason for this trend can be found with reference to Table 16 and Fig. 4 for ^{7}LiF TLDs, where $f(T_{\gamma})$ increases as the sleeve (Z/A) decreases to (Z/A) for ^{7}LiF ((Z/A) ratios for TLDs and sleeves are illustrated in Tables 8 and 9). Similar trends are observed for CaF_2:Mn TLDs as shown in Table 17 and Fig. 5. The mass energy absorption coefficients, however, increase with increasing sleeve atomic number (Fig. 3) in this energy range, owing to the fact that σ(photo) increases rapidly with increasing sleeve atomic number at low gamma energies. In this energy range, therefore, the TLD absorbed dose increases with increasing sleeve atomic number. This rapid rise of the mass energy absorption coefficient with decreasing gamma-ray energy in the high Z materials is also reflected in the increasing magnitude of the exponential attenuation factors (column (5)). Calculated TLD absorbed doses, corrected for exponential attenuation of the primary gamma ray in the sleeve material, are listed in column (6). The effect of these large attenuation corrections on the C/E ratios for lead, tantalum and tin in this energy range will be discussed in Section 4.5 for both types of TLDs.

The experimental results obtained in this investigation are presented in the next section.

4.4 Experimental Results for ^{7}LiF and CaF_2:Mn TLDs

The mean value of the measured TLD responses for all sleeve materials, ${}_{m}E^{exp}_{D(M)}$, together with their standard errors, are reported in Tables 18-23 for each gamma ray source. Procedures used to obtain these TLD responses are described in Section 3.13. Individual TLD responses were corrected for background, and the mean TLD response, together with its standard error, was determined for each type of sleeve encapsulation, in accordance with Eqs. (3.2) and (3.3). These results are reported in column (4) for each gamma-ray source. Individual TLD responses, corrected for background were divided by their corresponding sensitivity correction factors (Tables B.1 and B.2, Appendix B), and the mean TLD response, together with its standard error, was reported for each sleeve material. These sorted responses are reported in column (3) for each gamma-ray source.

The same TLD-sleeve combination was used for all source irradiations. The sensitivity correction factors used, therefore, remained the same for each encapsulated TLD irradiated by all gamma-ray sources. In a few instances, TLDs whose surfaces had become contaminated during use were replaced by other TLDs in the precision subset with similar sensitivity correction factors.

In most cases, the experimental results (sorted and unsorted values) closely resemble the trend observed in the calculated results, namely, that the encapsulated TLD response increased with increasing sleeve atomic number for each gamma-ray energy, except for the stainless steel sleeve. Recall from Section 4.3 that the atomic number of stainless steel is within 3% of the atomic number for iron. The ${}_{m}E^{calc}_{D(M)}$ results for stainless steel and iron were within 1% of each other, and this relationship is also evident in the sorted TLD responses in column (3).

Prior to calculating C/E ratios, presented in the next section, the calculated and experimental results were normalized to the corresponding results for the TLD encased by the reference material (see Equations (4.6)-(4.8)). A suitable reference material would have the least variation of $f(T_\gamma)$ as a function of gamma-ray energy, over the energy range under investigation. With reference to Tables 16 and 17, it is seen that aluminum exhibits the least variation in $f(T_\gamma)$ in this energy range. The results for both ^{7}LiF and CaF_2:Mn TLDs were therefore normalized to the results for aluminum encased TLDs.

4.5 Comparison of Theory and Experiment

Normalized C/E ratios, for each energy gamma-ray, are presented in Tables 24-29 as a function of sleeve material. Some significant trends were noted in these results for both TLD materials. C/E ratios were nominally close to unity for all sleeve materials irradiated with the highest energy gamma-ray (T_γ = 0.662 MeV). This was also the case

for the lower Z materials (all materials excluding lead and tantalum) irradiated at all gamma-ray energies. For the other combinations of sleeve materials and gamma-ray energies, i.e., high Z materials of lead and tantalum at low gamma-ray energies, significant deviations from unity were observed in the results. Factors contributing to these trends are discussed in this section.

Recall from the discussion of the calculated absorbed doses in the TLD material (Section 4.3) that the exponential attenuation factors increased rapidly with decreasing gamma-ray energy for the high Z materials. The effect of this large correction, due to sleeve attenuation, is clearly evident in the ^{51}Cr source results for both types of TLDs (Tables 26 and 29). For the lead and tantalum sleeves, it was observed that the simple exponential correction, based upon the mass energy absorption coefficients, was not adequate to reduce the C/E ratios to unity.

The effect of an error in the mass energy absorption coefficients for the lead sleeves at T_γ = 0.320 MeV (^{51}Cr source) can also be deduced from Tables 26 and 29. A reduction of 10% in the energy absorption coefficient of lead at this energy would reduce the C/E ratio for the sorted and unsorted TLDs with exponential attenuation by as much as 7%. Systematic errors in the energy absorption coefficients for the low Z materials, however, are unlikely to affect the C/E ratios since normalization to the aluminum sleeve would have

a cancelling effect on these errors. For the high Z materials, this cancelling effect is likely to be less pronounced.

The effect of the sensitivity correction factors can be deduced from the C/E ratios for sorted and unsorted TLDs at each gamma energy. The random errors associated with the unsorted TLD C/E ratios were nominally 3% for the ^{7}LiF and CaF_2:Mn TLDs. This random error was reduced to nominally 2% for the sorted C/E ratios.

The thickness of the sleeves used also influenced the results. Recall from the discussion in Section 2.2.1 that a sleeve thickness comparable to the range of the most energetic electron produced in the wall would be sufficient to satisfy the electronic equilibrium requirement. At T = 0.4 MeV, however, the sleeve thicknesses were much larger than the range of the most energetic electron (refer to Table 1). For example, in the case of the lead sleeve, the sleeve thickness was nominally 3 times as great as the electron range at this energy. This excessive thickness used may have resulted in a smaller TLD response due to scattering of the primary gamma-ray flux in the lead sleeve.

4.6 Intercomparisons of KSU Results with ANL Results

The C/E ratios for a 10 mCi ^{137}Cs source, obtained at ANL, are illustrated in Tables 31 and 32, respectively, for ^{7}LiF and CaF_2:Mn TLDs. The stainless steel sleeve was used for normalization purposes to obtain the results for ^{7}LiF TLDs in Table 31. Stainless steel was

selected because the aluminum sleeves used at ANL and KSU were of a different thickness. For comparison purposes, KSU data were also normalized to stainless steel. These results are illustrated in Table 30. Similar experimental procedures were used at ANL and KSU. However, a lucite sheet was used at ANL to support the source and TLDs during irradiation. Also, new TLDs were used at ANL, whereas the KSU TLDs had been used previously. As shown in Table 33 for ^{7}LiF TLDs, the ANL and KSU C/E values were within 10% of each other.

Normalized ANL C/E ratios for CaF_2:Mn TLDs irradiated by a ^{137}Cs gamma-ray source are shown in Table 32. These values can be directly compared to the KSU C/E ratios in Table 27. ANL data were not available for the tin, iron and stainless steel sleeves. For all other sleeves, the ANL and KSU data were in agreement within 5% (refer to Table 34).

Table 8. Partial compilation of input parameter used to calculate the dose ratio $f(T_\gamma)$ using TERC/III for 1x1x6 mm ^7LiF and CaF_2 TLDs.

Material	<Z/A>*	Density ρ(g/cm^3)	Mean Chord Length, g (g/cm^2)+	Ionization Potential, I (eV)#	Density Effect Parameters				
					c	a	m	x_0	x_1
^7LiF	0.4614	2.63	0.2430	86,5	-3.07	0.456	2.76	-0.07	2.0
CaF_2	0.4867	3.04	0.2806	158	-4.50	0.100	3.40	0.08	3.0

*Calculated using the equation: $\langle Z/A\rangle = \sum_j \varepsilon_j (Z_j/A_j)$.

For ^7LiF: $\varepsilon_1 = 0.269$, $Z_1 = 3$, $A_1 = 7$, $\varepsilon_2 = 0.731$, $Z_2 = 9$, and $A_2 = 18.9984$

For CaF_2: $\varepsilon_1 = 0.513$, $Z_1 = 20$, $A_1 = 40.08$, $\varepsilon_2 = 0.487$, $Z_2 = 0$, and $A_2 = 18.9984$

+$g = 4V\rho/S$ (g/cm^2)

#$\ln I = (Z/A)^{-1} \sum_j \varepsilon_j (Z_j/A_j) \ln I_j$

Table 9. Partial compilation of input parameters used to calculate the dose ratio $f(T_\gamma)$ using TERC/III for each encasement material.

Material	Atomic Number Z	Atomic Weight A	Ionization Potential I (eV)	Density Effect Parameters				
				c	a	m	X_0	X_1
Lead	82	207.2	826.	-6.21	0.355	2.64	0.4	3.0
Tantalum	73	180.9	701	-6.03	0.028	3.91	0.30	4.0
Tin	50	118.7	517	-6.28	0.404	2.52	0.20	3.0
Copper	29	63.57	323	-4.43	0.109	3.39	0.20	3.0
Iron	26	55.84	273	-4.62	0.127	3.29	0.10	3.0
Stainless Steel	25.23*	54.98+	273#	-4.62	0.127	3.29	0.10	3.0
Aluminum	13	27	164	-4.21	0.091	3.51	0.05	3.0

*$Z = \sum_j E_j Z_j$ where $E_j \equiv$ fraction by weight of the jth element

+$A = \sum_j E_j A_j$

#$\ln I = (Z/A)^{-1} \sum_j E_j (Z_j/A_j) \ln I_j$

Table 10. $_{m}E^{calc}_{D(M)}$ values for ^{137}Cs source (T_γ = 0.662 MeV) and ^{7}LiF TLDs for all sleeve materials.

Sleeve Type (1)	$_{m}E^{calc}_{D(M)}$ No. Attenuation $(\frac{\mu_{en}}{\rho})$ x $f(T_\gamma)$ (2)	$(\frac{\mu_{en}(T_\gamma)}{\rho})$ (cm^2/g) (3)	Sleeve Thickness t (g/cm^2) (4)	$\exp(\frac{\mu_{en}(T_\gamma)}{\rho} xt)$ (5)	$_{m}E^{calc}_{D(M)}$ With Attenuation (6)
Lead	.04468	.06444	.734	1.048	.04263
Tantalum	.03955	.05262	.696	1.037	.03813
Tin	.03172	.03296	.608	1.020	.03109
Copper	.02872	.02793	.694	1.020	.02817
Stainless Steel	.02851	.02805	.693	1.020	.02824
Iron	.02840	.02808	.656	1.019	.02788
Aluminum	.02762	.02821	0.514	1.015	.02722

Table 11. $_{m}E^{calc}_{D(M)}$ values for ^{198}Au source (T_γ = .4118 MeV) and ^{7}LiF TLDs for all sleeve materials.

Sleeve Type	$_{m}E^{calc}_{D(M)}$ No Attenuation $(\frac{\mu_{en}}{\rho}) \times f(T_\gamma)$	$(\frac{\mu_{en}(T_\gamma)}{\rho})$ $(\frac{cm^2}{g})$	Sleeve Thickness t (g/cm^2)	$\exp(\frac{\mu_{en}}{\rho}(T_\gamma)\, xt)$	$_{m}E^{calc}_{D(M)}$ With Attenuation
(1)	(2)	(3)	(4)	(5)	(2)/(5)
Lead	.05093	.13808	.734	1.10666	.04602
Tantalum	.04397	.10706	.696	1.07736	.04081
Tin	.03281	.05058	.608	1.03123	.03182
Copper	.02866	.03106	.694	1.02179	.02805
Stainless Steel	.02841	.03020	.693	1.02115	.02782
Iron	.02835	.03019	.656	1.02000	.02779
Aluminum	.02766	.02866	.514	1.01484	.02726

Table 12. $_{m}E^{calc}_{D(M)}$ values for ^{51}Cr source (T_{γ} = 0.320 MeV) and ^{7}LiF TLDs for all sleeve materials.

Sleeve Type	$_{m}E^{calc}_{D(M)}$ No Attenuation $(\frac{\mu_{en}(T_{\gamma})}{\rho}) \times f(T_{\gamma})$	$\frac{\mu_{en}(T_{\gamma})}{\rho}$ $(\frac{cm^2}{g})$	t $(\frac{g}{cm^2})$	$\exp(\frac{\mu_{en}(T_{\gamma})}{\rho} xt)$	$_{m}E^{calc}_{D(M)}$ With Attenuation
(1)	(2)	(3)	(4)	(5)	(2)/(5)
Lead	.05719	.23596	.734	1.18909	.04810
Tantalum	.04873	.18256	.696	1.13549	.04292
Tin	.03420	.07677	.608	1.04778	.03264
Copper	.02828	.03512	.694	1.02467	.02760
Stainless Steel	.02787	.03275	.693	1.02296	.02723
Iron	.02785	.03289	.656	1.02181	.02726
Aluminum	.02698	.02813	.514	1.05625	.02554

Table 13. $_{m}E^{calc}_{D(M)}$ values for ^{137}Cs source (T_γ = 0.662 MeV) and CaF_2:Mn TLDs for all sleeve materials.

Sleeve Type	$_{m}E^{calc}_{D(M)}$ No. Attenuation $(\frac{\mu_{en}(T_\gamma)}{\rho}) \times f(T_\gamma)$	$\frac{\mu_{en}(T_\gamma)}{\rho}$ $(\frac{cm^2}{g})$	Sleeve Thickness t $(\frac{g}{cm^2})$	$\exp(\frac{\mu_{en}(T_\gamma)}{\rho} \times t)$	$_{m}E^{calc}_{D(M)}$ With Attenuation
(1)	(2)	(3)	(4)	(5)	(2)/(5)
Lead	.04314	.06444	.734	1.04844	.04115
Tantalum	.03879	.05263	.696	1.03731	.03739
Tin	.03210	.03295	.608	1.02024	.03146
Copper	.02953	.02795	.694	1.01959	.02896
Stainless Steel	.02934	.02805	.693	1.01963	.02822
Iron	.02925	.02808	.656	1.01859	.02872
Aluminum	.02860	.02821	.514	1.01461	.02819

Table 14. $_{m}E^{calc}_{D(M)}$ values for ^{198}Au source (T_{γ} = 0.4118 MeV) and CaF_2:Mn TLDs for all sleeve materials.

Sleeve Type	$_{m}E^{calc}_{D(M)}$ No Attenuation $(\frac{\mu_{en}(T_{\gamma})}{\rho}) \times f(T)$	$(\frac{\mu_{en}(T_{\gamma})}{\rho})$ cm^2/g	Sleeve Thickness t $(\frac{g}{cm^2})$	$\exp(\frac{\mu_{en}(T_{\gamma})}{\rho} \times t)$	$_{m}E^{calc}_{D(M)}$ With Attenuation
(1)	(2)	(3)	(4)	(5)	(2)/(5)
Lead	.04880	.13880	.734	1.10667	.04410
Tantalum	.04298	.10706	.696	1.07736	.03989
Tin	.03361	.05058	.608	1.03123	.03259
Copper	.03013	.03105	.694	1.02178	.02949
Stainless Steel	.02989	.03020	.693	1.02117	.02927
Iron	.02984	.03019	.656	1.02000	.02925
Aluminum	.02927	.02863	.514	1.01482	.02884

Table 15. $_{m}E^{calc}_{D(M)}$ values for ^{51}Cr source (T_γ = 0.320 MeV) and CaF_2:Mn TLDs for all sleeve materials.

Sleeve Type	$_{m}E^{calc}_{D(M)}$ No Attenuation $\frac{\mu_{en}(T_\gamma)}{\rho} \times f(T_\gamma)$	$\frac{\mu_{en}(T_\gamma)}{\rho}$ $(\frac{cm^2}{g})$	Sleeve Thickness t $(\frac{g}{cm^2})$	exp((3)x(4))	$_{m}E^{calc}_{D(M)}$ With Attenuation
(1)	(2)	(3)	(4)	(5)	(2)/(5)
Lead	.05464	.23598	.734	1.18911	.04595
Tantalum	.04760	.18265	.696	1.13556	.04192
Tin	.03545	.07678	.608	1.04779	.03383
Copper	.03040	.03512	.694	1.02467	.02967
Stainless Steel	.03004	.03275	.693	1.02296	.02976
Iron	.03003	.03289	.656	1.02181	.02931
Aluminum	.02929	.02813	.514	1.01456	.02887

Table 16. Variation of $f(T_\gamma)$ with gamma-ray energy for encapsulated ^{7}LiF TLDs (from TERC/III code).

Sleeve	$f(T_\gamma)$		
	^{137}Cs T_γ = 0.662 MeV	^{198}Au T_γ = 0.4118 MeV	^{51}Cr T_γ = 0.320 MeV
Pb	.69336	.36884	.24237
Ta	.75162	.41070	.26693
Sn	.96238	.64868	.44549
Cu	1.02828	.92273	.80524
Fe	1.01140	.93905	.84676
S.S.	1.01640	.94073	.85099
Al	.97909	.96511	.95912

Table 17. Variation of $f(T_\gamma)$ with gamma-ray energy for encapsulated CaF_2:Mn TLDs.

Sleeve	$f(T_\gamma)$		
	^{137}Cs T_γ = 0.662 MeV	^{198}Au T_γ = 0.4118 MeV	^{51}Cr T_γ = 0.32010 MeV
Pb	.66946	.35159	.23155
Ta	.73703	.40146	.26061
Sn	.97420	.66449	.46171
Cu	1.05653	.97037	.86560
S.S.	1.04599	.98974	.91725
Fe	1.04167	.98841	.91304
Al	1.01382	1.02235	1.04124

Table 18. ^{7}LiF TLD readouts for various sleeve encapsulations and a ^{137}Cs gamma ray source (T_{γ} = 0.662 MeV).

Sleeve Type (1)	Number of Sleeves N (2)	Sorted Readouts $m^{E^{exp}_{D(M)}} \pm \frac{\sigma_M}{\sqrt{N}}$ (3)	Unsorted Readouts $m^{E^{exp}_{D(M)}} \pm \frac{\sigma_M}{\sqrt{N}}$ (4)
Lead	9	4.523 ± .035	4.704 ± .029
Tantalum	10	4.188 ± .026	4.301 ± .026
Tin	15	3.343 ± .025	3.304 ± .025
Copper	14	3.018 ± .029	3.048 ± .030
Stainless Steel	17	2.950 ± .020	2.865 ± .021
Iron	15	2.931 ± .016	2.927 ± .018
Aluminum	7	2.900 ± .044	2.966 ± .042

Table 19. ^{7}LiF readouts for various sleeve encapsulations and ^{198}Au *gamma ray source* (T_{γ} = 0.4118 MeV).

Sleeve Type (1)	Number of Sleeves (N) (2)	Sorted Readouts $m_{E_{D(M)}}^{exp} \pm \frac{\sigma_M}{\sqrt{N}}$ (3)	Unsorted Readouts $m_{E_{D(M)}}^{exp} \pm \frac{\sigma_M}{\sqrt{N}}$ (4)
Lead	9	2.516 ± .071	2.604 ± .072
Tantalum	8	2.154 ± .096	2.211 ± .095
Tin	10	1.736 ± .074	1.717 ± .073
Copper	14	1.486 ± .048	1.503 ± .050
Stainless Steel	17	1.573 ± .046	1.524 ± .047
Iron	16	1.488 ± .032	1.486 ± .033
Aluminum	5	1.469 ± .041	1.499 ± .043

Table 20. ^{7}LiF readouts for various sleeve encapsulations and a ^{51}Cr gamma ray source (T_{γ} = 0.320 MeV).

Sleeve Type (1)	Number of Sleeves (N) (2)	Sorted Readouts $m^{E}_{D(M)}^{exp} \pm \frac{\sigma_M}{\sqrt{N}}$ (3)	Unsorted Readouts $m^{E}_{D(M)}^{exp} \pm \frac{\sigma_M}{\sqrt{N}}$ (4)
Lead	9	1.603 ± .017	1.660 ± .017
Tantalum	10	1.565 ± .013	1.610 ± .013
Tin	14	1.329 ± .010	1.301 ± .008
Copper	12	1.015 ± .008	1.014 ± .011
Stainless Steel	16	1.038 ± .008	1.006 ± .008
Iron	16	1.005 ± .006	1.003 ± .006
Aluminum	8	0.950 ± .012	0.977 ± .009

Table 21. CaF_2:Mn readouts for various sleeve encapsulations and ^{137}Cs gamma-ray source (T_γ = 0.662 MeV).

Sleeve Type	Number of Sleeves (N)	Sorted Readouts $m E^{exp}_{D(M)} \pm \frac{\sigma_M}{\sqrt{N}}$	Unsorted Readouts $m E^{exp}_{D(M)} \pm \frac{\sigma_M}{\sqrt{N}}$
(1)	(2)	(3)	(4)
Lead	9	4.838 ± .035	5.054 ± .034
Tantalum	10	4.570 ± .040	4.737 ± .039
Tin	14	4.121 ± .022	4.063 ± .021
Copper	12	3.475 ± .034	3.519 ± .034
Stainless Steel	16	3.691 ± .024	3.532 ± .032
Iron	16	3.686 ± .018	3.679 ± .019
Aluminum	8	3.432 ± .031	3.527 ± .029

Table 22. CaF_2:Mn readouts for various sleeve encapsulations and ^{198}Au gamma ray source (T_γ = 0.4118 MeV).

Sleeve Type	Number of Sleeves (N)	Sorted Readouts $m E^{exp}_{D(M)} \pm \frac{\sigma_M}{\sqrt{N}}$	Unsorted Readouts $m E^{exp}_{D(M)} \pm \frac{\sigma_M}{\sqrt{N}}$
(1)	(2)	(3)	(4)
Lead	9	.923 ± .015	.964 ± .018
Tantalum	10	.836 ± .009	.866 ± .010
Tin	14	.711 ± .003	.701 ± .003
Copper	14	.648 ± .003	.656 ± .003
Stainless Steel	17	.690 ± .008	.663 ± .007
Iron	16	.644 ± .004	.643 ± .004
Aluminum	8	.642 ± .006	.659 ± .006

Table 23. CaF_2:Mn TLD readouts for all sleeve encapsulation materials and ^{51}Cr gamma ray source (T_γ = 0.3201 MeV).

Sleeve Type (1)	Number of Sleeves (N) (2)	Sorted Readouts $m^{E^{exp}_{D(M)}} \pm \frac{\sigma_M}{\sqrt{N}}$ (3)	Unsorted Readouts $m^{E^{exp}_{D(M)}} \pm \frac{\sigma_M}{\sqrt{N}}$ (4)
Lead	9	3.943 ± .036	4.119 ± .037
Tantalum	10	3.847 ± .032	3.988 ± .033
Tin	14	3.487 ± .019	3.426 ± .016
Copper	14	2.899 ± .015	2.913 ± .026
Stainless Steel	17	2.923 ± .013	2.805 ± .011
Iron	16	2.880 ± .013	3.426 ± .016
Aluminum	8	2.693 ± .023	2.768 ± .023

Table 24. Comparison of theory with experiment for encapsulated ^{7}LiF TLDs exposed to a nominal 3 mCi ^{137}Cs source (T_{γ} = 0.662 MeV). Data normalized to aluminum.

Sleeve Type	No. of Sleeves Irradiated	C/E Sorted TLDs		C/E Unsorted TLDs	
		With Attenuation Correction	Without Attenutation Correction	With Attenuation Correction	Without Attenuation Correction
Pb	9	1.004 ± 0.027	1.037 ± 0.028	0.987 ± 0.024	1.020 ± 0.025
Ta	10	0.970 ± 0.023	0.991 ± 0.024	0.965 ± 0.022	0.988 ± 0.015
Sn	15	0.990 ± 0.017	0.996 ± 0.017	1.025 ± 0.018	1.031 ± 0.017
Cu	14	0.994 ± 0.019	0.999 ± 0.019	1.007 ± 0.018	1.012 ± 0.018
S.S.	17	1.009 ± 0.017	1.014 ± 0.017	1.063 ± 0.016	1.068 ± 0.017
Fe	15	1.013 ± 0.017	1.017 ± 0.017	1.038 ± 0.016	1.042 ± 0.016
Al	7	1.000 ± 0.015	1.000 ± 0.015	1.000 ± 0.020	1.000 ± 0.020

Table 25. Comparison of theory with experiment for encapsulated ^{7}LiF TLDs exposed to a nominal 3 mCi ^{198}Au source (T_{γ} = 0.4118 MeV). Data normalized to aluminum.

Sleeve Type	No. of Sleeves	C/E Sorted TLDs		C/E Unsorted TLDs	
		With Attenuation Correction	Without Attenuation Correction	With Attenuation Correction	Without Attenuation Correction
Pb	9	0.986 ± 0.039	1.075 ± 0.043	0.972 ± 0.039	1.060 ± 0.042
Ta	8	1.021 ± 0.054	1.084 ± 0.057	1.015 ± 0.052	1.078 ± 0.056
Sn	10	0.988 ± 0.050	1.004 ± 0.051	1.019 ± 0.052	1.036 ± 0.053
Cu	14	1.017 ± 0.043	1.024 ± 0.044	1.026 ± 0.045	1.033 ± 0.045
S.S.	17	0.953 ± 0.039	0.959 ± 0.039	1.004 ± 0.042	1.010 ± 0.043
Fe	16	1.006 ± 0.035	1.012 ± 0.036	1.029 ± 0.037	1.034 ± 0.038
Al	5	1.000 ± 0.039	1.000 ± 0.039	1.000 ± 0.041	1.000 ± 0.041

Table 26. Comparison of theory with experiment for encapsulated ^{7}LiF TLDs exposed to a nominal 3 mCi ^{51}Cr source (T_{γ} = 0.320). Data normalized to aluminum.

Sleeve Type	No. of Sleeves Irradiated	C/E Sorted TLDs		C/E Unsorted TLDs	
		With Attenuation Correction	Without Attenuation Correction	With Attenuation Correction	Without Attenuation Correction
Pb	9	1.116 ± 0.018	1.257 ± 0.021	1.108 ± 0.015	1.248 ± 0.017
Ta	10	1.020 ± 0.015	1.099 ± 0.017	1.020 ± 0.012	1.096 ± 0.013
Sn	14	0.914 ± 0.013	0.906 ± 0.014	0.960 ± 0.011	0.952 ± 0.011
Cu	12	1.011 ± 0.015	0.981 ± 0.015	1.041 ± 0.015	1.010 ± 0.015
S.S.	16	0.976 ± 0.015	0.945 ± 0.014	1.035 ± 0.013	1.003 ± 0.013
Fe	16	1.009 ± 0.014	0.976 ± 0.014	1.040 ± 0.010	1.005 ± 0.011
Al	8	1.000 ± 0.018	1.000 ± 0.018	1.000 ± 0.009	1.000 ± 0.009

Table 27. Comparison of theory with experiment for encapsulated CaF_2:Mn TLDs exposed to a nominal 3 mCi ^{137}Cs source (T_γ = 0.662 MeV). Data normalized to aluminum.

Sleeve Type	No. of Sleeves Irradiated	C/E Sorted TLDs		C/E Unsorted TLDs	
		With Attenuation Correction	Without Attenuation Correction	With Attenuation Correction	Without Attenuation Correction
Pb	9	1.036 ± .012	1.070 ± 0.012	1.019 ± .011	1.053 ± .011
Ta	10	.996 ± .013	1.019 ± 0.013	0.988 ± .011	1.010 ± .012
Sn	14	.929 ± .010	.935 ± .010	.969 ± .010	.974 ± .010
Cu	14	1.015 ± .014	1.020 ± .014	1.040 ± .013	1.035 ± .013
S.S.	17	.931 ± .011	.954 ± .011	1.000 ± .012	1.024 ± .013
Fe	16	.949 ± .010	.952 ± .010	.977 ± .010	.980 ± .010
Al	8	1.000 ±0.013	1.000 ± 0.013	1.000 ± .012	1.000 ±0.012

Table 28. Comparison of theory with experiment for encapsulated CaF_2:Mn TLDs exposed to a nominal 3 mCi ^{198}Au source (T_γ = 0.4118 MeV). Data normalized to Al.

Sleeve Type	No. of Sleeves Irradiated	C/E Sorted TLDs		C/E Unsorted TLDs	
		With Attenuation Correction	Without Attenuation Correction	With Attenuation Correction	Without Attenuation Correction
Pb	9	1.063 ± .020	1.159 ± .022	1.045 ± .020	1.140 ± .022
Ta	10	1.062 ± .015	1.128 ± .016	1.053 ± .015	1.117 ± .016
Sn	14	1.020 ± .010	1.036 ± .010	1.062 ± .011	1.079 ± .011
Cu	14	1.013 ± .013	1.020 ± .013	1.028 ± .010	1.035 ± .010
S.S.	17	.944 ± .014	.950 ± .014	1.009 ± .014	1.015 ± .014
Fe	16	1.011 ± .011	1.016 ± .011	1.039 ± .012	1.045 ± .012
Al	8	1.000 ± .013	1.000 ± .013	1.000 ± .013	1.000 ± .013

Table 29. Comparison of theory with experiment for encapsulated CaF_2:Mn TLDs exposed to a nominal 3 mCi ^{51}Cr source. (T_γ = 0.320 MeV). Data normalized to Al.

Sleeve Type	No. of Sleeves	C/E Sorted TLDs		C/E Unsorted TLDs	
		With Attenuation Correction	Without Attenuation Correction	With Attenuation Correction	Without Attenuation Correction
Pb	9	1.087 ± .014	1.273 ± .016	1.069 ± .013	1.254 ± .015
Ta	10	1.016 ± .009	1.138 ± .010	1.008 ± .012	1.128 ± .013
Sn	14	.905 ± .009	.937 ± .009	.947 ± .009	.978 ± .009
Cu	14	0.955 ± .010	.964 ± .010	.977 ± .012	.986 ± .012
S.S.	17	.950 ± .009	.945 ± .009	1.017 ± .009	1.012 ± .007
Fe	16	.949 ± .009	.959 ± .009	.978 ± .009	.987 ± .010
Al	8	1.000 ± .017	1.000 ± .017	1.000 ± .017	1.000 ± .017

Table 30. Comparison of theory with experiment for encapsulated ^{7}LiF TLDs exposed to a nominal 3 mCi ^{137}Cs source (T_{γ} = 0.662 MeV). Data normalized to stainless steel.

Sleeve	No. of Sleeves Irradiated	C/E Sorted TLDs		C/E Unsorted TLDs	
		With Attenuation Correction	Without Attenuation Correction	With Attenuation Correction	Without Attenuation Correction
Pb	9	.994 ± .028	1.022 ± .029	.929 ± .009	.955 ± .009
Ta	10	.960 ± .034	.978 ± .034	.980 ± .008	.925 ± .009
Sn	15	.982 ± .018	.981 ± .018	.965 ± .010	.964 ± .010
Cu	14	.984 ± .019	.985 ± .019	.964 ± .012	.947 ± .012
S.S.	17	1.000 ± .024	1.000 ± .024	1.000 ± .010	1.000 ± .010
Fe	15	1.002 ± .023	1.003 ± .023	.975 ± .010	.976 ± .010
Al	7	.991 ± .022	.986 ± .022	.941 ± .015	.936 ± .015

Table 31. Comparison of theory with experiment for encapsulated ^{7}LiF TLDs exposed to a nominal 10 mCi ^{137}Cs source (data taken at Argonne National Laboratory, normalized to stainless steel).

Sleeve Type	C/E Sorted TLDs	
	With Attenuation	Without Attenuation
Pb	1.080 ± .030	1.050 ± .029
Ta	1.034 ± .030	1.016 ± 0.30
Sn	.947 ± .029	.946 ± .029
Cu	.974 ± .028	.974 ± .028
S.S.	1.000 ± .031	1.000 ± .031
Fe	.994 ± .031	.995 ± .031

Table 32. Comparison of theory with experiment for encapsulated CaF_2:Mn TLDs exposed to a nominal 10 mCi ^{137}Cs source (data taken at Argonne National Laboratory, May 1977, normalized to aluminum).

Sleeve Type	No. of Sleeves Irradiated	C/E Sorted TLDs		C/E Unsorted TLDs	
		With Attenuation Correction	Without Attenuation Correction	With Attenuation Correction	Without Attenuation Correction
Pb	19	.994 ± .010	1.021 ± .008	.984 ± .008	1.017 ± .008
Ta	17	.984 ± .009	1.007 ± .009	.986 ± .009	1.008 ± .009
Sn	-	-	-	-	-
Cu	28	.981 ± .009	.986 ± .009	.988 ± .008	.993 ± .008
S.S.	-	-	-	-	-
Fe	-	-	-	-	-
Al	20	1.000 ± .010	1.000 ± 0.010	1.000 ± .010	1.000 ± .010

Table 33. Intercomparison of C/E ratios of KSU data and ANL data for ^{137}Cs source and ^{7}LiF TLDs. (Data referenced to stainless steel.)

Sleeve Type	ANL/KSU Sorted TLDs
Pb	1.087 ± .043
Ta	1.077 ± .049
Sn	.964 ± .034
Cu	.990 ± .027
S.S.	1.000 ± .039
Fe	.992 ± .039

Table 34. Intercomparison of C/E ratios of KSU data and ANL data for ^{137}Cs source and CaF_2:Mn TLDs. (Data referenced to aluminum)

Sleeve Type	ANL/KSU Sorted TLDs	ANL/KSU Unsorted TLDs
Pb	.954 ± .013	.966 ± .013
Ta	.988 ± .016	.998 ± .014
Sn	-	-
Cu	.967 ± .016	.959 ± .014
S.S.	-	-
Fe	-	-
Al	1.000 ± .016	1.000 ± .016

5.0 CONCLUSIONS

Sufficient data were collected in this investigation to characterize the energy response of encapsulated ^{7}LiF and CaF_2:Mn TLDs for a variety of electron equilibrium sleeves, in the energy range 0.3-0.7 MeV. Comparisons were made with the theoretical TLD responses predicted by the TERC/III code, which used as a basis the theoretical development of Burlin (8) for intermediate-sized cavities. Several approximations were made in the theory behind the TERC/III code. It was assumed, for example, that the volume averaged electron spectrum could be represented as the weighted sum of the electron distributions characteristic of the sleeve and dosimeter materials, that bremsstrahlung and delta ray production could be ignored, and electrons slow down continuously in these materials. Also, the theoretical model could only be as accurate as the input data used. The C/E ratios served as a useful tool in the validation of the theoretical model in the energy range under investigation.

The results obtained showed that consistent, reproducible TLD responses are obtainable with the experimental procedures outlined in Chapter 3. The use of sensitivity selection, to select and use a precision subset from a batch of TLDs, restricted the random errors to within 3% for both types of TLDs. Using sensitivity correction factors to correct individual TLD responses

resulted in a further reduction of the random errors to within 2% in most cases.

The C/E ratios obtained were nominally unity for all sleeves at the highest gamma-ray energy (T_γ = 0.662 MeV) and for low Z materials at low gamma-ray energies. Significant deviations from unity were obtained for the reverse condition of gamma-ray energy and sleeve material, i.e., low gamma-ray energy and high Z materials. Some factors that may have produced these trends are:

(1) Inaccuracies in the mass energy absorption coefficients. Any systematic errors in these coefficients would cancel out for low Z materials at all gamma-ray energies, due to normalization of the results to the aluminum sleeve. For high Z materials, at low gamma-ray energies, this cancelling effect would not be as pronounced.

(2) Inadequacy of the exponential attenuation model. The exponential attenuation correction is inadequate (i.e., under corrects) for the high Z materials at low gamma-ray energies.

(3) Excessive sleeve thickness at low gamma ray energies. For all sleeve materials, the sleeve thicknesses used were much greater than the maximum electron range at T_γ = 0.3 MeV, resulting in errors due to scattering of the primary gamma-ray flux in the sleeves. These errors resulted in an absorbed dose in the dosimeter that was less than if electronic equilibrium had existed in the sleeves.

6.0 SUGGESTIONS FOR FURTHER STUDY

Future investigations in the field should concentrate on the following areas:

(1) The effect of sleeve thickness on the C/E ratios at low gamma-ray energies. This would complement the requirement for charged particle equilibrium.

(2) The accuracy of the continuous slowing down approximation of the electron spectrum at gamma-ray energies below 0.3 MeV.

(3) The use of a different type of model, other than exponential, to describe sleeve attenuation at low gamma-ray energies in high Z materials.

(4) The effect of the use of total attenuation coefficients, rather than mass energy absorption coefficients, on the C/E ratios.

7.0 ACKNOWLEDGEMENTS

The author wishes to express his sincerest gratitude to Dr. Gale Simons for his patient and considerate guidance throughout the duration of this investigation, and in the preparation of this thesis (not forgetting an uncountable number of precious weekends!). Thanks are extended to Shelly Kemnitz for her excellent and prompt typing of the manuscript, and to the faculty and students of the Nuclear Engineering Department for their friendly and cooperative attitude. Gratitude is extended to the Nuclear Engineering Department for their financial support of this research.

REFERENCES

1. Gray, L. H., "The Absorption of Penetrating Radiation," Proc. Roy. Soc., A122, 647 (1929).

2. Gray, L. H., "An Ionization Method for the Absolute Measurement of Gamma Ray Energy," Proc. Roy. Soc., A156, 578 (1936).

3. Laurence, G. C., "The Measurement of Extra Hard X-Rays and Gamma Rays in Roentgens," Can. J. Res., A15, 67 (1937).

4. Spencer, L. V., and Attix, F. H., "A Theory of Cavity Ionization," Radiation Res., 3, 239 (1955).

5. Burch, P. R. J., "Cavity Ion Chamber Theory," Radiation Res., 4, 361 (1955).

6. N. C. R. P., "Stopping Powers for Use With Cavity Chambers," National Committee on Radiation Protection and Measurements," National Bur. Std. (U.S.), Handbook 79 (1961).

7. Daniels, F., Boyd, C. A., and Saunders, D. F., Science 117, 343 (1953).

8. Burlin, T. E., "A General Theory of Cavity Ionization," Brit. J. Radiol. 39, 727-734 (1966).

9. Burlin, T. E., "The Measurement of Exposure Dose for High Energy Radiation with Cavity Ionization Chambers," Phys. Med. Biol., 3, 197 (1959).

10. Burlin, T. E., "An Experimental Examination of Theories Relating the Absorption of Gamma-Ray Energy in a Medium to the Ionization Produced in a Cavity," Phys. Med. Biol., 11, 255-266 (1961).

11. Burlin, T. E., Ph.D. Thesis, University of London (1962).

12. Burlin, T. E., "The Limits of Validity of Cavity Ionization Theory," British J. Radiol., 35, 343 (1962).

13. Burlin, T. E., "Exposure Dose Measurements," Phys. Med. Biol., 7, 241 (1962).

14. Burlin, T. E., "Further Examination of Theories Relating the Absorption of Gamma-Ray Energy in a Medium to the Ionization Produced in a Cavity," Phys. Med. Biol., 11, 255-266 (1966).

15. Burlin, T. E., and Chan, F. K., "The Effect of the Wall on the Fricke Dosimeter," Int. J. of App. Rad. and Iso., 20, 767-775 (1969).

16. Stanford, G. S., and Johnson, T. W., "Determination of Gamma-Ray Heating in a Critical Facility by Thermoluminescent Dosimetry," ANL-7373 (1968).

17. Adamson, J., Absalom, R. M., Baker, A. B., Ingram G., Pattenden, S. K. I., and Stevenson, J. M., "ZEBRA-6; Dilute Plutonium-Fueled Assembly," ANL-7320, 216-230 (1966).

18. Simons, G. G., "Thermoluminescent Dosimetry Applied to Gamma Ray Dose Measurements in Critical Assemblies," ANL-7710, (289-294) (1971).

19. Simons, G. G. and Yule, T. J., "Gamma Ray Heating Measurements in Zero Power Fast Reactors with Thermoluminescent Dosimeters," Nucl. Sci. and Engg., 53, 2, 162-175 (1974).

20. Simons, G. G. and Olson, A. P., "Analyses and Measurements of Gamma-Ray Heating in the Demonstration Benchmark Plutonium-Fueled Critical Assembly," Nucl. Sci. and Engg., 53, 2, 176-196 (1974).

21. Attix, F. H. and Roesch, W. C., Radiation Dosimetry, Vol. 1, 2nd Ed., Academic Press, New York and London, Chapter 8 (1968).

22. Attix, F. H., Roesch, W. C., and Tochilin, E., Radiation Dosimetry Vol. 2, 2nd Ed., Academic Press, New York and London, Chapter 11 (1966).

23. Boag, J. W., "Ionization Chambers," Radiation Dosimetry, Vol. II, Attix, H., and Roesch, W. H., ed., Page 6 (1966).

24. Evans, R. D., The Atomic Nucleus, McGraw Hill, New York (1955).

25. Laurence, G. C., "The Measurement of Extra Hard X-Rays and Gamma Rays in Roentgens," Can. J. Res., A15, 67 (1937).

26. Attix, F. H., DeLa Vergne, L., and Ritz, V. H., "Cavity Ionization as a Function of Wall Material," J. Res. Natl. Bur. Std., 60, 235 (1958).

27. Katz, L., and Penfold, A., Revs. of Modern Physics, 24, 28 (1952).

28. Simons, G. G. and Emmons, L. L., "Evaluation of Gamma-Ray Response Calculations for ^{7}LiF TLDs," Nuclear Instruments and Methods (in press) (1979).

29. Schwinert, P. A. and Driscoll, M. J., "Gamma Heating Measurements in Fast Breeder Reactor Blankets," AEC Research and Development Report, Massachusetts Institute of Technology, Cambridge, Massachusetts (1974).

30. Burgkhardt, B., Henera, R., and Piesch, E., "Long-Term Fading Experiment with Different TLD Systems," International Conference in Luminescence Dosimetry, Sao Paolo, Brazil (1977) page 75.

31. Burke, Gail de Planque, "Compilation of Available Studies on TLD Stability," International Conference in Luminescence Dosimetry, Sao Paolo, Brazil (1977) page 84.

32. Martin, M. J., and Blichert-Toft, P. H. Nuclear Data Tables, A8, 1970.

33. Cameron, J. R., Suntharalingam, N., and Kenney, G. N., Thermoluminescent Dosimetry, The University of Wisconsin Press (1968).

34. Bevington, P. R., Data Reduction and Error Analysis for the Physical Sciences, McGraw Hill, New York, Chapter 4 (1969).

35. Berger, M. J., and Seltzer, S. M., "Tables of Energy Losses and Ranges of Electrons and Positrons," NASA-SP-3012 (1964).

36. Simons, G. G. and Emmons, L. L., "Experimental Evaluation of a Model for Calculating the Gamma-Ray Response of Encapsulated Solid State Dosimeters," ZPR-TM-238, Argonne National Laboratory (1976).

37. Storm, Ellery, and Israel, Harvey, "Photon Cross Sections from 1 keV to 100 MeV for Elements Z = 1 to Z = 100", Nuclear Data Tables, A-7 (1970).

APPENDIX A: Flow Chart for the SAD code (sensitivity selection).

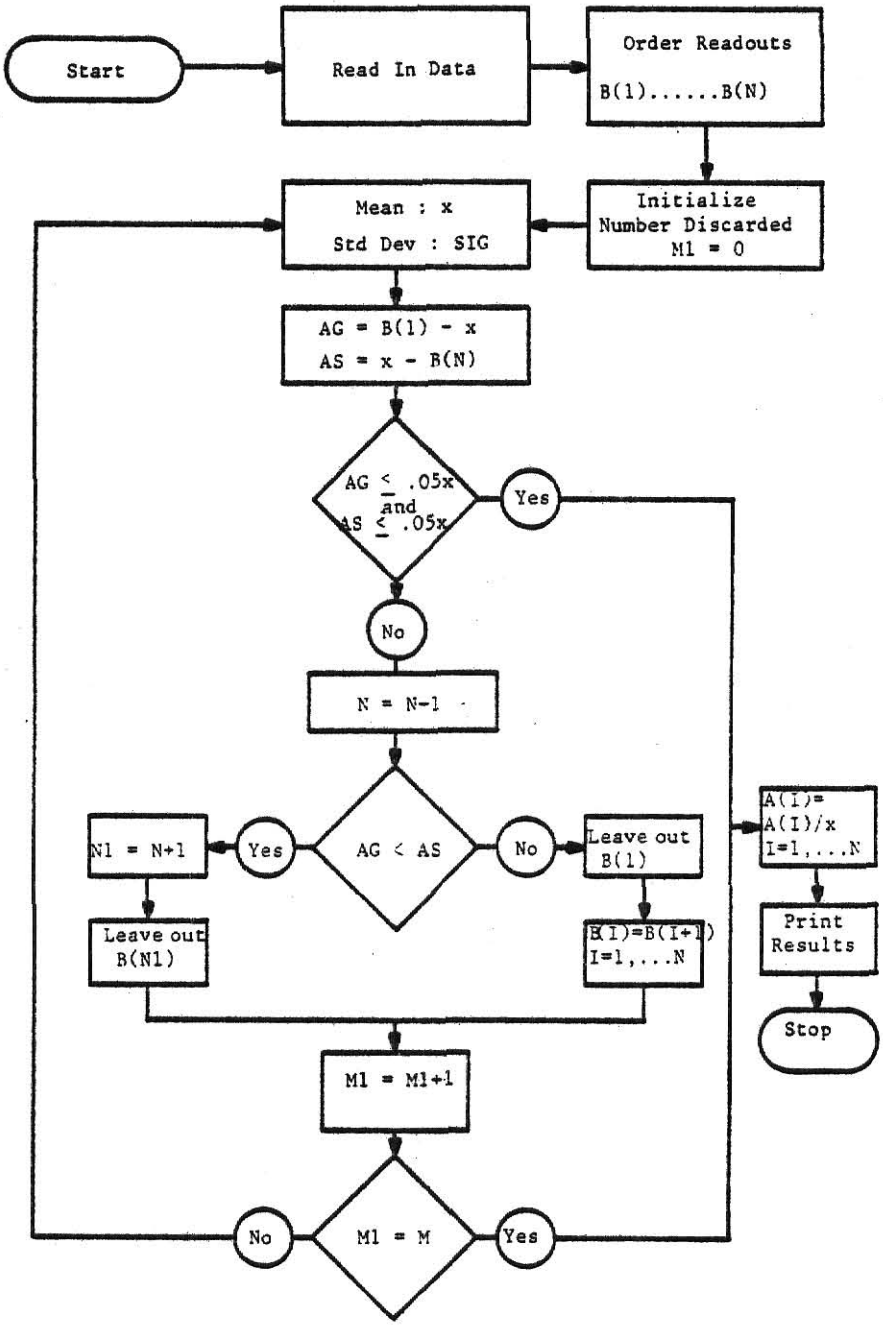

Appendix B

This appendix contains the sensitivity correction factors used for the sorted encapsulated ^{7}LiF and CaF_2:Mn TLDs. Sensitivity correction factors for each type TLD were obtained from the SAD code (Section 3.12, Chapter 3), and the values presented here are for the precision subset.

Table. B.1. Sensitivity correction factors (obtained from the SAD code, Section 3.12) used for encapsulated ^{7}LiF TLDs irradiated by all gamma-ray sources.

Sleeve Encapsulation	Sleeve Number	TLD Number	Sensitivity Correction Factor
	1	68	1.0374
	2	84	1.0368
	3	52	1.0368
Lead	4	67	1.0363
	5	8	1.0357
	6	108	1.0347
	7	83	1.0347
	8	74	1.0347
	9	116	1.0314
	2	36	1.0309
	5	60	1.0293
	6	89	1.0287
	9	45	1.0287
	10	50	1.0282
Tantalum	11	146	1.0277
	13	39	1.0266
	14	43	1.0250
	16	25	1.0234
	18	121	1.0228
	6	179	.9910
	7	100	.9905
	9	79	.9905
	10	87	.9900
	11	154	.9894
	12	135	.9894
Tin	13	140	.9889
	15	80	.9889
	16	134	.9884
	17	171	.9873
	19	92	.9867
	20	115	.9862
	22	152	.9857
	24	109	.9857
	23	222	.9851

Table B.1 - continued

Sleeve Encapsulation	Sleeve Number	TLD Number	Sensitivity Correction Factor
Copper	6	49	1.0180
	11	90	1.0174
	12	70	1.0169
	13	31	1.0131
	15	24	1.0131
	16	200	1.0115
	18	185	1.0104
	19	34	1.0099
	21	202	1.0094
	22	123	1.0094
	23	122	1.0094
	24	2	1.0083
	25	37	1.0067
	26	73	1.0061
Stainless Steel	400	97	.9770
	401	218	.9765
	402	158	.9765
	403	147	.9760
	404	182	.9749
	405	220	.9738
	406	211	.9738
	407	78	.9722
	408	131	.9711
	409	102	.9711
	410	124	.9706
	411	210	.9695
	412	86	.9695
	413	184	.9679
	414	120	.9625
	415	142	.9620
	418	128	.9620
Iron	4	107	1.0034
	5	69	1.0034
	6	125	1.0029
	7	88	1.0029
	9	81	1.0018
	10	212	1.0002
	12	144	.9997
	13	99	.9997
	14	151	.9991
	15	72	.9959
	18	57	.9959
	19	15	.9959
	20	114	.9943

Table B.1 - continued

Sleeve Encapsulation	Sleeve Number	TLD Number	Sensitivity Correction Factor
Iron	22	27	.9943
	25	148	.9921
	29	66	.9916
Aluminum	5	180	1.0217
	6	111	1.0217
	7	163	1.0207
	8	129	1.0207
	9	104	1.0185
	11	209	1.0180
	12	194	1.0180

Table B.2. Sensitivity Correction factors for the precision subset of encapsulated CaF_2:Mn TLDs.

Sleeve Material	Sleeve Number	TLD Number	Sensitivity Correction Factor
Lead	1	93	1.0460
	2	86	1.0460
	3	77	1.0460
	4	76	1.0460
	5	36	1.0460
	6	34	1.0460
	7	164	1.0424
	8	89	1.0424
	9	83	1.0424
Tantalum	2	85	1.0387
	5	70	1.0387
	6	49	1.0387
	9	13	1.0387
	10	167	1.0351
	11	163	1.0351
	13	101	1.0351
	14	94	1.0351
	16	92	1.0351
	18	75	1.0351
Tin	6	185	.9881
	7	160	.9881
	9	158	.9881
	10	153	.9881
	11	142	.9881
	12	137	.9881
	13	136	.9881
	15	115	.9881
	16	183	.9884
	17	131	.9884
	19	212	.9808
	20	209	.9808
	22	143	.9808
	24	139	.9808
	23	118	.9808

Table B.2 - continued

Sleeve Material	Sleeve Number	TLD Number	Sensitivity Correction Factor
Copper	6	147	1.0170
	11	126	1.0170
	12	90	1.0170
	13	174	1.0134
	15	168	1.0134
	16	135	1.0134
	18	121	1.0134
	19	106	1.0134
	21	80	1.0134
	22	188	1.0098
	23	122	1.0098
	24	114	1.0098
	25	102	1.0098
	26	170	1.0062
Iron	4	84	1.0062
	5	182	1.0025
	6	116	1.0025
	7	113	1.0025
	9	103	1.0025
	10	192	.9989
	12	130	.9989
	13	99	.9989
	14	184	.9953
	15	176	.9953
	18	171	.9953
	19	169	.9953
	20	155	.9953
	22	110	.9953
	25	162	.9917
	29	152	.9917
Stainless Steel	400	151	.9663
	401	129	.9663
	402	72	.9663
	403	199	.9627
	404	179	.9627
	405	154	.9627
	406	120	.9627
	407	214	.9591
	408	198	.9591
	409	197	.9591

Table B.2 - continued

Sleeve Material	Sleeve Number	TLD Number	Sensitivity Correction Factor
Stainless Steel	410	194	.9591
	411	191	.9591
	412	189	.9591
	413	178	.9591
	414	157	.9591
	415	149	.9591
	418	145	.9591

GAMMA-RAY ENERGY RESPONSE OF ENCAPSULATED ^{7}LiF AND CaF_2:Mn THERMOLUMINESCENT DOSIMETERS

by

KRISHNAN LAKSHMINARAYAN

B. Tech., Indian Institute of Technology
Madras, INDIA, 1974

AN ABSTRACT OF A MASTER'S THESIS

submitted in partial fulfillment of the

requirements for the degree

MASTER OF SCIENCE

Department of Nuclear Engineering
KANSAS STATE UNIVERSITY
Manhattan, Kansas

1980

ABSTRACT

Sufficient data were collected in this investigation to characterize the energy response of encapsulated ^{7}LiF and CaF_2:Mn TLDs for a variety of electron equilibrium sleeves, in the energy range 0.3-0.7 MeV. Well-established procedures developed at the Argonne National Laboratory were used to obtain consistent, reproducible results. Experimental results obtained were compared to the theoretical predictions from the TERC/III code, which employed Burlin's development for intermediate-sized cavities. The C/E ratios computed for each gamma ray energy revealed the following trends: C/E ratios were nominally close to unity for all sleeves irradiated by the highest gamma-ray energy (T_γ = 0.662 MeV), and for the low Z sleeve materials at lower gamma-ray energies. Significant deviations from unity were reported for the reverse combination of gamma-ray energy and sleeve material, i.e., for low gamma-ray energies and high Z sleeve materials.